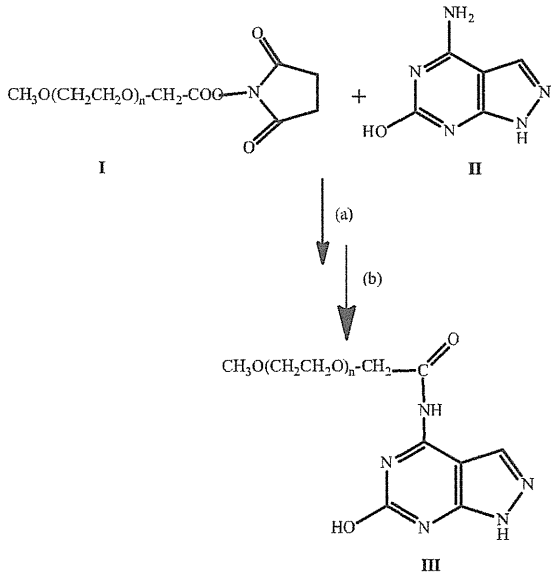

Scheme 1. Synthetic scheme for synthesis of mono-AHPP-PEG conjugate. 0.1 M NaOH, $CHCl_3$, 0°C, pH 9.0; 0.1 M HCl, room temperature, pH 1.5.

solubilized, spontaneously formed micelles. The solution was then subjected to gel chromatography with Sephadex G-100 Fine column (Ø1.5 × 87 cm) (Amersham Biosciences AB, Uppsala, Sweden); Elution peaks corresponding to absorption of AHPP-PEG conjugate at 270 nm was collected, lyophilized and used for further analysis.

Synthesis of bis-(AHPP)-PEG conjugate

As depicted in the reactions Scheme 2, bis-(AHPP)-PEG synthesis was carried out via two-step processes, involving activation of PEG with 4-nitrophenyl chloroformate using a method reported (Varonese et al. 1985; Varonese et al. 2005), followed by interfacial reaction with AHPP. Briefly, to a solution of 5.0 g (2.5 mmol) PEG in 20 mL dry dimethylformamide (DMF), 1.3 g (6.4 mmol) of 4-nitrophenyl chloroformate was added by several aliquots. After stirring this reaction mixture at room temperature for 24 h, 250 mL of dry diethyl ether was added to precipitate the product. The precipitates were then collected by filtration and washed three times with diethyl ether, and the residue was redissolved in acetonitrile:ethylether (1:3 v/v). The product was allowed to precipitate at 4°C for 2 h. Finally, the activated PEG was collected by filtration and dried under vacuum (yield 4.8 g). Further, bis-(AHPP)-PEG was synthesized following the same protocol as used above to synthesis of mono-AHPP-PEG. Yield of bis-(AHPP)-PEG obtained was 1.39 g (91.4%).

Gel filtration chromatography of AHPP-PEG micelles

For purification and characterization of AHPP-PEG micelles, gel chromatography with Sephadex G-100 superfine (Amersham Biosciences AB, Uppsala, Sweden) was performed by using column of Ø1.5 × 87 cm, eluted with 0.1 M bicarbonate pH 8.2. Each eluted 3.1 mL fractions were monitored by UV absorption at 270 nm, and peak fractions were collected followed by dialysis and lyophilized. The lyophilized powder thus obtained was subjected to further characterization by UV-visible and FTIR spectroscopy. To estimate the apparent molecular size of the AHPP-PEG conjugates the size exclusion chromatography was performed using various known molecular weight globular proteins as reference standards.

Dynamic light scattering (DLS)

DLS studies were carried out with a Photal DLS-7000 HLs laser-light scattering spectrophotometer (Otsuka Electronics, Osaka, Japan), equipped with a 10 mW He-Ne (632.5 nm) laser light source. For DLS measurements, the scattering angle was fixed at 90° and the temperature of the sample was maintained at 25.0 ± 0.01°C. Particle size determination was carried out using samples at concentration of 2.5 mg/mL prepared in 0.15 M NaCl/0.01 M sodium phosphate buffer (pH 7.4), which yielded the optimal counts.

UV-visible spectroscopy

UV/visible absorption spectra were recorded on a spectrophotometer (Model UV/Vis-550, JASCO Corp., Tokyo, Japan). The drug concentration was quantified using absorption at 270 nm, based on a standard curve for free AHPP in 0.1 M NaOH (by further diluting 100–10 μM with buffer at pH 8.5).

Fourier transform infrared (FTIR) spectroscopy

Fourier transform infrared (FTIR) spectra were recorded on a FT/IR-4200 spectrometer (JASCO Corp., Tokyo, Japan) using KBr discs. The KBr discs were prepared using Jasco MP-1 minipress unit.

Fluorescence spectroscopy

Fluorescence spectra were recorded on F-2500 fluorescence spectrophotometer (Hitachi, Tokyo). The sample solutions of AHPP and AHPP-PEG conjugates were excited at 270.0 nm (corresponding to λmax of AHPP) and emission for fluorescence from 280.0 to 500.0 nm were measured.

Elemental analysis

Analysis of the AHPP-PEG conjugates after purification by Sephadex column chromatography and drying over P_2O_5 for three days in vacuum were carried out for hydrogen, carbon and nitrogen.

Quantification of amino group after PEGylation by 2,4,6-trinitrobenzendsulfonic acid (TNBS) and fluorescamine assay

The degree of PEG conjugation to AHPP was measured by quantifying the primary amino group by the TNBS (Stocks et al. 1986) with modifications. AHPP, mono-AHPP-PEG and bis-(AHPP)-PEG (for details see Figure 5A) were dissolved in 0.01 M NaOH and further diluted to

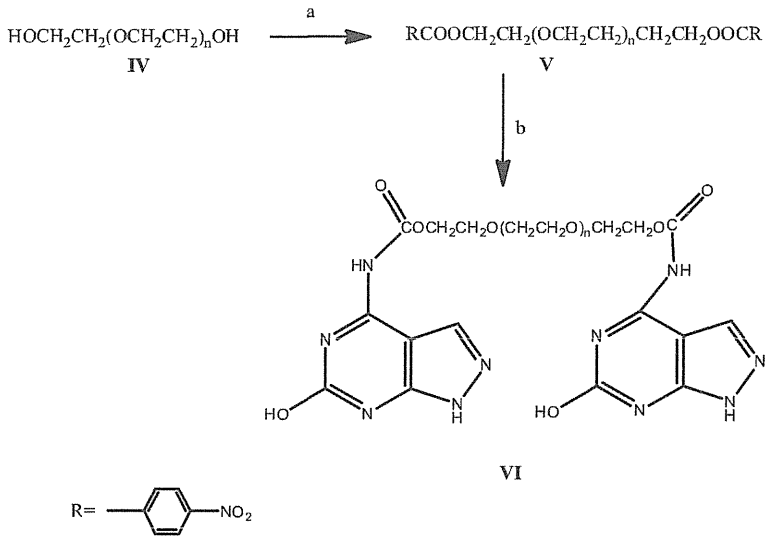

Scheme 2. Synthetic scheme for synthesis of bis-(AHPP)-PEG conjugate. (a) 4-nitrophenyl chloroformate, DMF, 25°C; (b) AHPP, chloroform, 25°C.

final concentrations with 0.1 M borate buffer (pH 8.0). Then, 0.1 mL of 0.1 M TNBS (Wako Pure Chemicals, Osaka) solution was added and vortexed for five minutes. Their absorbances were recorded at 355.0 nm. Moreover, quantification of amino groups was also carried out by use of fluorescamine (4-phenylspiro[furan-2(3H)-1′-phthalan]-3,3′-dione) assay. Briefly, solutions of AHPP and AHPP-PEG conjugates were prepared with a final concentration of 1.0–8.0 μM/mL by serial dilutions using 0.1 M borate buffer (pH 8.0), and 0.5 mL of fluorescamine (Wako Pure Chemicals, Osaka) solution (0.3 mg/mL in acetone) was added. The mixture was vortexed for 2 min and the fluorescence was measured using a florescence spectrophotometer (F-2500, Hitachi High-Technology Corp., Tokyo); excitation at 390.0 nm was used and emission at 475.0 nm was measured.

Release of AHPP-PEG conjugate from its micelle

The release of AHPP-PEG conjugate from the micelles *in vitro* was verified by placing the micellar solutions (2.0 mg in 1.0 mL of 0.2 M phosphate buffer) in sealed dialysis tubes (Mw cut-off 10,000; Spectapor, Spectrum Laboratories, San Diego, CA). The sealed dialysis tubes were submerged in 35.0 mL of (i) pH 6.0 of 0.2 M phosphate buffer; (ii) pH 7.4 of 0.2 M phosphate buffer, and (iii) pH 9.0, 0.2 M carbonate buffers. The dialysis bags were then incubated with reciprocal shaking of the dialysis bath at 1 Hz for several hours at 37°C. The release from the dialysis bags were quantified spectroscopically by measuring absorbance at 270 nm.

Measurement of XO activity and inhibition by AHPP-PEG conjugates

Formation of uric acid from xanthine was measured by absorbance at 290 nm with upon addition of xanthine oxidase (XO). Briefly, AHPP and xanthine were dissolved in 0.1 M NaOH at first, and then diluted with 10 mM sodium phosphate buffer (pH 7.4) final concentration of about 100 μM. Bovine milk XO stock (23 unit /mL, Sigma-Aldrich) was diluted to 330 mU/mL with phosphate buffer (pH 7.4) and further diluted to 1.5 mU/mL. Cuvette containing 1.5 mU/mL of XO (final concentration) in 10 mM sodium phosphate buffer (pH 7.5), graded amounts of xanthine, mono-AHPP-PEG and bis-(AHPP)-PEG, respectively, were added to start the reaction (for details see Figure 8). The velocity of uric acid formation at 25°C was determined as evidenced by the increase in absorbance at 290 nm.

In vivo *pharmacokinetics of AHPP-PEG micelles*

Male ddY mice of 6-week were used in the pharmacokinetics study of AHPP-PEG conjugates. mono-AHPP-PEG and bis-(AHPP)-PEG (dissolved in physiological saline) or free AHPP (dissolved in 0.01 M NaOH) was injected intravenously (i.v.) at 10 mg/kg (AHPP equivalent). After scheduled intervals, mice were killed and blood was collected in the presence of heparin. Then, 100 μL of plasma obtained by centrifugation (3500 rpm for 20 min) was diluted with 850 μL of saline and 50 μL of trichloroacetic acid was added to precipitate plasma proteins. The precipitated plasma proteins was removed by centrifuge (3000 rpm for 15 min) and 500 μL supernatant was diluted with 1.5 mL of saline and fluorescence was measured by fluorescence spectrophotometer at 270 nm excitation (corresponding to AHPP) and peak emission at 356.0 nm.

Results

Synthesis and characterizations of AHPP-PEG micelles

In the first method, mono-AHPP-PEG was synthesized using NOF PEG (ME-20 AS) which resulted in a water-soluble derivate of AHPP. In the second method, an

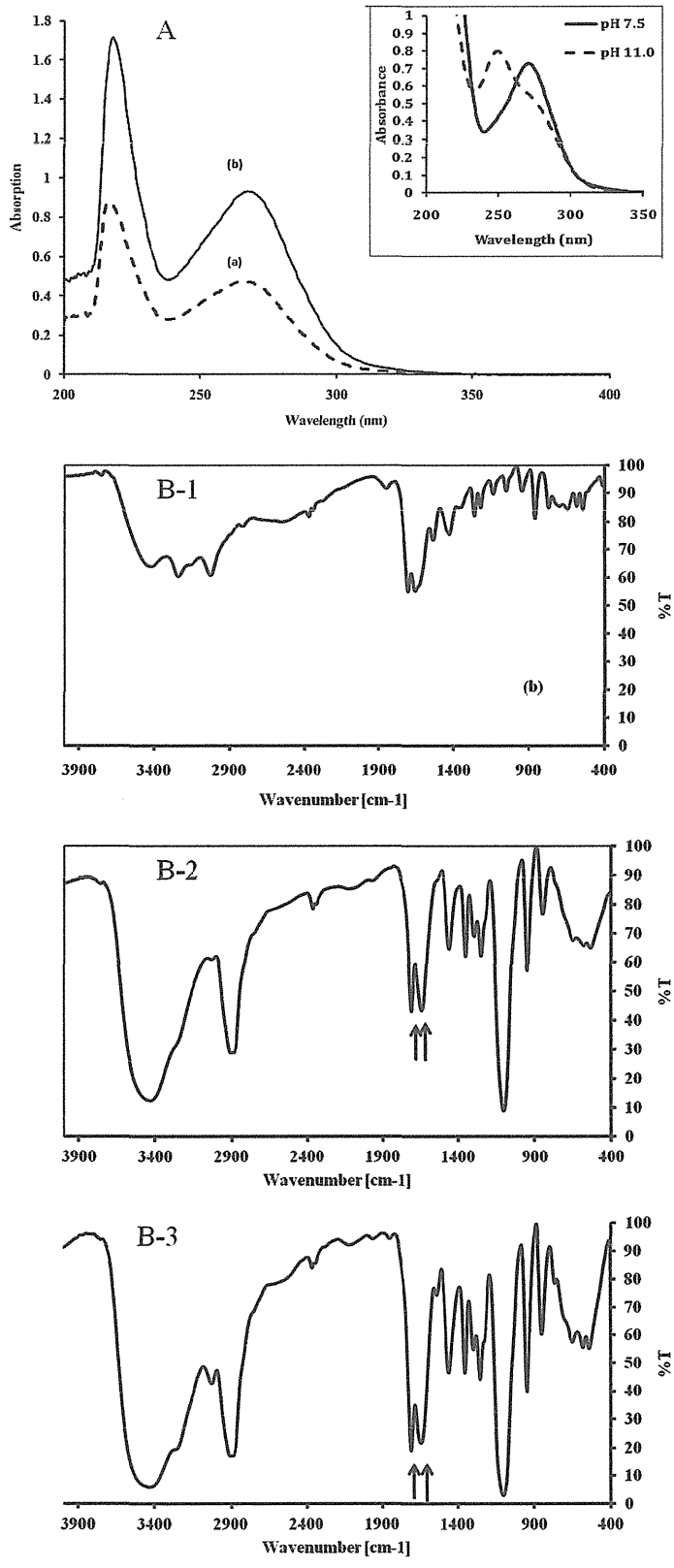

Figure 2. Characterization of AHPP-PEG micellar conjugates. (A) UV-vis spectroscopy of mono-AHPP-PEG (a) and bis-(AHPP)-PEG (b) in 0.025 M NaOH, concentrations used; 0.05 mg/mL. Inset image is for the UV absorption spectrum of AHPP. The λ_{max} for AHPP undergoes a bathochromic shift from 270 nm (pH 7.5) to 254.0 nm (pH 11.0). (B) FTIR spectrums of (B-1) AHPP; (B-2) mono-AHPP-PEG; and (B-3) bis-(AHPP)-PEG in KBr discs. The peak of AHPP becomes broader at 3400 cm^{-1} compared to AHPP-PEG due to large–NH stretching. The peak at about 1000 cm^{-1} is due to C-C stretching of PEG chain. The arrow indicates amide (B-2) and carbamate (B-3) peak.

activated PEG derivative was first synthesized employing PEG derivative of an active carbonate of *p*-nitorophenyl-chloroformate as described in Scheme 2. Both conjugates exhibited good water solubility up to 50 mg/mL (48 mM AHPP eqvt.), which is more than adequate concentration for dose escalation for clinical applications, and far greater than free AHPP (<0.05 mg/mL).

Characterization of AHPP-PEG conjugates

In both cases of AHPP-PEG conjugates, they were purified by Sephadex gel G-100 chromatography prior to their characterization by UV, IR spectroscopes. Figure 2A shows the UV-visible absorption spectra of mono-AHPP-PEG (a), and bis-(AHPP)-PEG (b), respectively. Free AHPP (Figure 2A, inset image) had a very strong absorption peak at 254 nm at higher pH 11.0, whereas at lower pH 7.5 the peak maxima shifted to 270 nm. The content of AHPP in the AHPP-PEG conjugates was calculated by specific UV absorption based on plotting a standard curve of free AHPP at pH 8.5 in 0.2 M phosphate buffer. In the elemental analysis, mono-AHPP-PEG conjugate showed a content of N, 2.84; C, 53.30; H, 8.51 and bis-(AHPP)-PEG conjugate showed N, 5.52; C, 52.39; H, 8.19; which is similar to the calculated value of N, 2.94; C, 53.50; H, 8.60 and N, 5.51; C, 52.90; H, 8.24 for mono-AHPP-PEG and bis-(AHPP)-PEG, respectively. As the PEG contains no nitrogen, the presence of nitrogen in AHPP-PEG micelles reflects the conjugation.

The extent of the reaction between primary amino groups of AHPP with activated PEG following the S_N2 type of reaction mechanism. Formation of AHPP-PEG conjugate between AHPP and PEG was confirmed by FTIR spectroscopy (Figure 2B). In FTIR spectrum, the N-H stretching of primary amine at 3350.0 cm^{-1} disappeared, and the peak at 1643.05 and 1708.6 cm^{-1} indicated the presence of–C=O groups, suggesting the conjugation of amine group of AHPP to the PEG.

Sephadex gel chromatography of AHPP-PEG conjugates

The calculated mean molecular weights based on chemical formula of PEG was mono-AHPP-PEG and

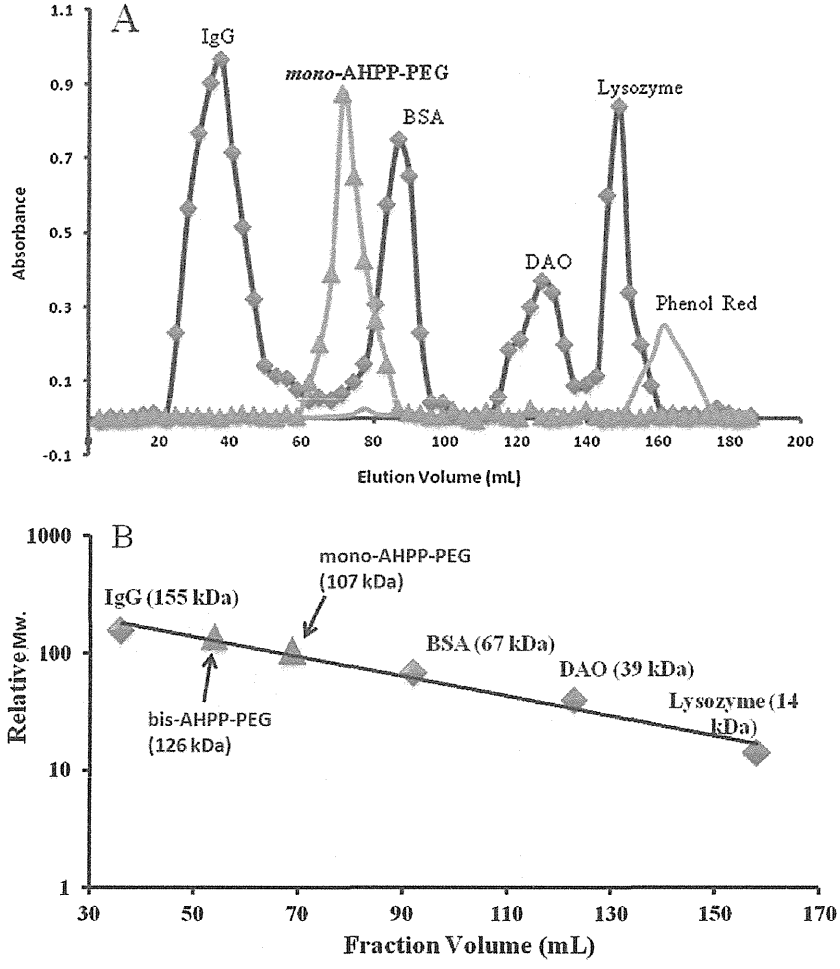

Figure 3. Sephadex G-100 purification and gel size exclusion chromatography of pegylated AHPP and standard proteins. (A) Standard proteins and AHPP-PEG conjugate. Detection wavelengths were 280.0 nm and 270.0 nm for standard proteins and AHPP-PEG conjugates, respectively. (B) Plot of relative molecular weight vs. fraction volume (mL) to determine the micellar size of AHPP-PEG conjugates.

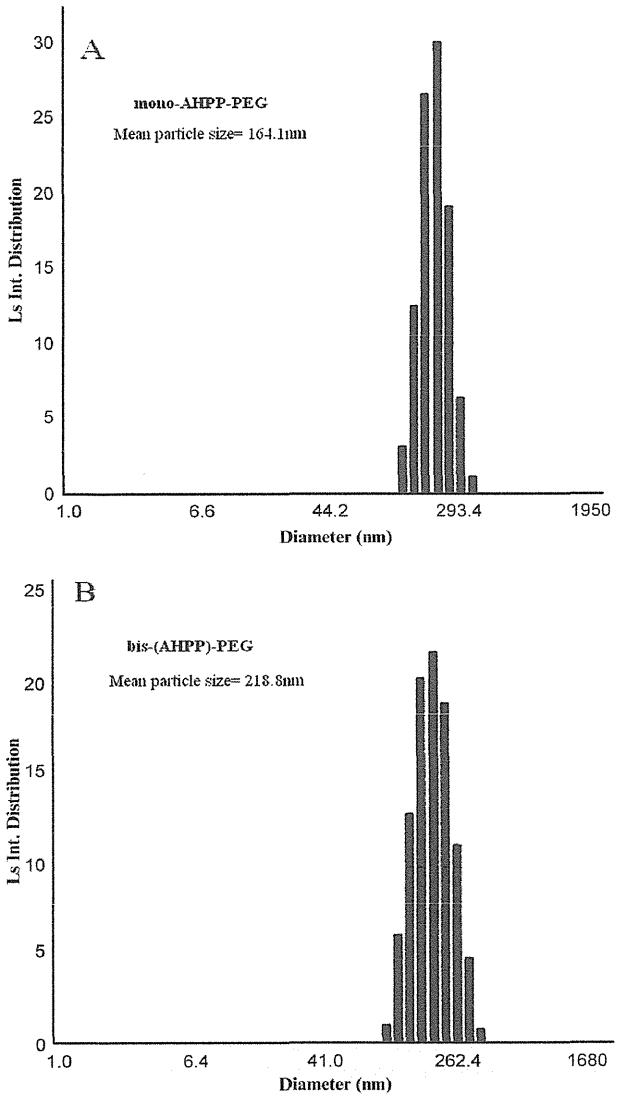

Figure 4. Dynamic light scattering (DLS) of pegylated AHPP micelles. The samples prepared in 0.15 M NaCl/0.01 M sodium phosphate buffer (pH 7.4). The average particle size of the micelles was 164.1 nm and 218.8 nm for (A) mono-AHPP-PEG and (B) bis-(AHPP)-PEG, respectively. Plot of Ls Int. Distribution vs. diameter was shown.

bis-(AHPP)-PEG conjugates are 2.2 and 2.3 kDa, respectively. However, Sephadex G-100 superfine (Amersham Biosciences AB, Uppsala, Sweden) high resolution gel chromatography showed a large apparent molecular sizes of 107 kDa and 126 kDa (Figure 3A), based on the standard proteins molecular weights markers [IgG, 155 kDa; bovine serum albumin (BSA), 67 kDa; lysozyme, 14 kDa] as shown in Figure 3B. These results indicates that, irrespective of the molecular size (2.2 kDa) of PEG chain, self-associate to form supramolecular assemblies in aqueous medium, similar to that reported earlier for several PEGylated micellar drugs and conjugates (Harada et al. 1999; Otsuka et al. 2003; Ideta et al. 2005; Veronese et al. 2005). The present result is also similar to that observed with the earlier preparation of polyethylene glycol-zinc protoporphyrin (PEG-ZnPP) and styrene-maleic acid copolymer-AHPP (SMA-AHPP) micelles in our laboratory using styrene-maleic acid (SMA) copolymer, where these conjugates shows large molecular size of about 116 kDa and 67 kDa, respectively, by Sephadex gel chromatography (Sahoo et al. 2002; Fang et al. 2009a). It is anticipated that these macromolecular conjugates are capable of utilizing the EPR effect for tumor selective delivery (Maeda et al. 2009b; Matsumera et al. 1886; Maeda et al. 2001c).

Solution behavior of the AHPP-PEG conjugates as analyzed by dynamic light scattering (DLS)

The micellar structure of the AHPP-PEG conjugates was further elaborated by DLS studies. The mono-AHPP-PEG and bis-(AHPP)-PEG micelles exhibited a mean particle size of 164.1 nm (Figure 4A) and 218.8 nm, respectively (Figure 4B). These are in line with the recently reported SMA-AHPP (Fang et al. 2009a) and PEG-ZnPP (Sahoo et al. 2002; Iyer et al. 2007b) micelles, which behave in a similar fashion forming self-assembled associations in aqueous solution. This result indicates that the micelles prepared by mono-AHPP-PEG conjugate have tighter interaction between PEG and AHPP resulting in smaller size of micelles than bis-(AHPP)-PEG. Moreover, there may be hydrophobic interaction among AHPP molecules as head group and PEG as hydrophilic tail (Nishide et al. 1977).

In addition, the results from gel chromatography showed a relatively smaller size than that of DLS. This is probably due to the interaction between AHPP-PEG and gel which resulting in a apparently smaller size, and it may thus not reflect the real size of AHPP-PEG micelle.

Quantification of amino group after conjugation with PEG

Loss of the primary amino group after reaction was quantified by two methods; (a) TNBS and (b) fluorescamine method. Degree of modification by TNBS was 87.47% and 91.2% for mono-AHPP-PEG and bis-(AHPP)-PEG conjugates respectively (Figure 5A). The fluorescamine assay results 88.22 and 93.98% for mono-AHPP-PEG and bis-(AHPP)-PEG conjugates respectively indicating most of the AHPP are reacted with polyethylene chains (Figure 5B).

Release of AHPP-PEG conjugate from the micelles

Because the AHPP-PEG is linked by covalent bond, free AHPP will not released in physiological condition. The release study is thus designed to investigate the release of AHPP-PEG conjugate from its micellar form. To support this notion, we found that no precipitation was observed both inside and outside the dialysis bag even after centrifugation because AHPP will precipitate in this condition if it is cleaved from AHPP-PEG. It is thus indicates that released AHPP is coupled with PEG.

As shown in Figure 6, very slow release rate was found in aqueous medium, about 1.1–1.2% per day for

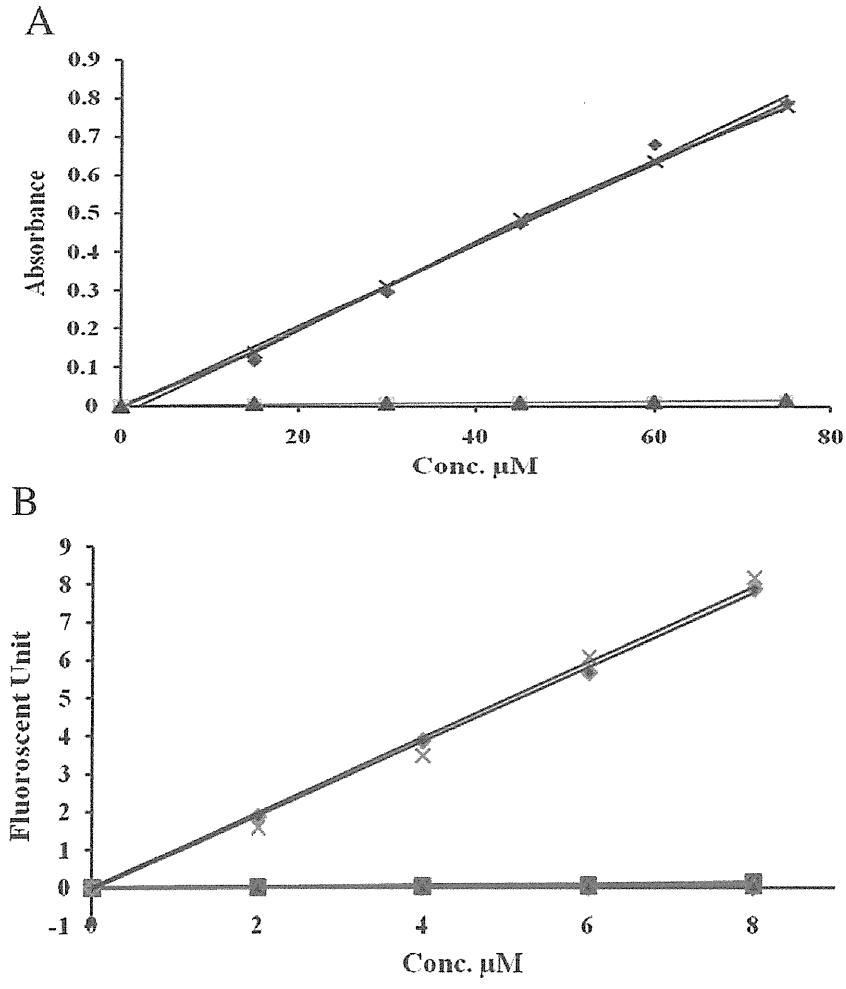

Figure 5. Quantification of amino groups and measurement of 3m Pegylation by (A) TNBS and (B) Fluoroscamine assay. (A) In TNBS assay absorbance was recorded at 355.0 nm corresponding to of λ_{max} of TNBS. (B) In fluorescamine assay sample solutions were excited at 390.0 nm was used and emission at 475.0 nm was measured corresponding to fluorescamine. Symbols: ♦ AHPP; X, mono-AHPP-PEG; ▲ bis-(AHPP)-PEG; ■ glycine.

the mono-AHPP-PEG (Figure 6A) and 1.5–1.6% per day for bis-(AHPP)-PEG (Figure 6B). Furthermore, the release below critical micellar concentration (CMC) level (0.3 mg/mL) was carried out and it was observed that below CMC level the release was fast i.e. almost 100% released within 3–4 h. Whereas, above CMC level the release was relatively slow i.e. 1.1–1.5%/day.

Stability studies of AHPP-PEG micelles

AHPP-PEG conjugates forms micelles in aqueous solutions, was further supported by a study using fluorescence spectroscopy. Namely, free AHPP in alkaline solution showed a strong fluorescence in 325–425 nm range upon excitation at 270.0 nm; however, when AHPP-PEG micelles dissolved in aqueous solutions, where it exists as densely packed form, the fluorescence of AHPP-PEG was almost quenched (Figure 7A) suggesting AHPP-PEG behaves as micellar structure, and the π–π interaction of AHPP quenches fluorescence due to energy transfer in the pack state as in micelle though in aqueous solution. Similar phenomena have been reported for the micellar drugs using SMA containing doxorubicin and pirarubicin in our previous work (Greish et al. 2004; Greish et al. 2005). Using fluorescence spectroscopy, we investigated the stability of AHPP-PEG micelles in various buffers with different pH 5.0–10.0. As shown in Figure 7B, the quenched states of fluorescence intensity of AHPP-PEG were observed over the range from pH 5.0 to 10.0, indicating the compact micellar structure is stable over a wide pH range.

The micellar stability and nature of AHPP-PEG conjugates in aqueous medium was further studied by fluorescence spectrophotometer and change of size of the micelles was monitored by DLS (figure 7C). When AHPP-PEG micelles were dissolved in distilled water or in neutral pHs up to pH 8.5 the integrity of micelles was conserved constant size at about 170 and 220 nm for mono-AHPP-PEG and bis-(AHPP)-PEG conjugates, respectively.

To study the stability of AHPP-PEG micelles under different pH conditions, or in presence of strong base, we

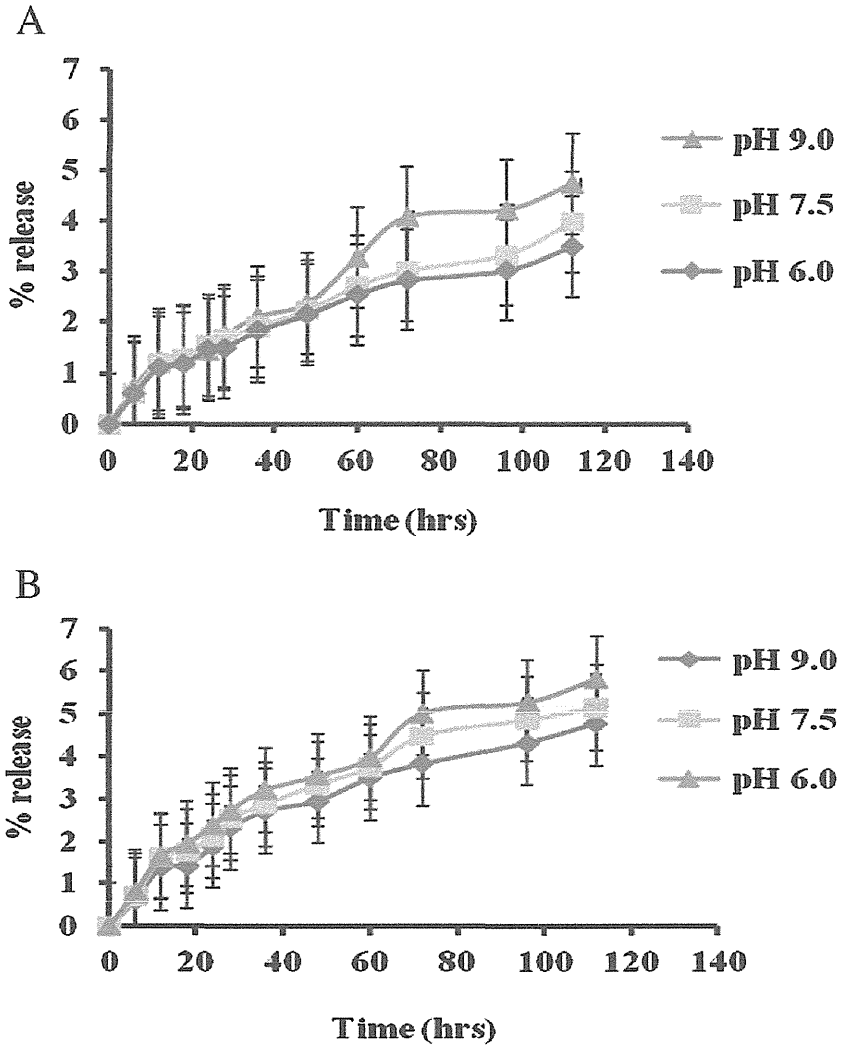

Figure 6. *In vitro* release from mono-AHPP-PEG (A) and bis-(AHPP)-PEG (B) conjugates. A constant release rate of ~1.2 and ~ 1.5% per day was observed at neutral pH for mono-AHPP-PEG and bis-(AHPP)-PEG, respectively. Release was quantified spectroscopically at 270.0 nm corresponding to AHPP was measured.

titrated the micellar solutions (1 mg/mL) against 0.1 M NaOH solutions, while monitoring the particle size by DLS and pH simultaneously (for details see Figure 7C). When 0.1 M NaOH was added drop wise into AHPP-PEG micellar solution (with increasing pH), it makes the micelles more and more unstable. At the end of titration, at pH 10.5 ± 0.1 units, the micellar size suddenly becomes very large ~1100 nm indicating the rupture or aggregation of micelle, corresponding to the inflection point in the curve (Figure 7). Both conjugates show similar stability and inflection point nearly at pH 10.5. Above the inflection point, we observed the disruption of micelles (burst effect), leading to an abrupt increase in the particle size.

Measurement of XO inhibitory activity by the AHPP-PEG conjugates

The initial velocity of uric acid formation was measured in the presence of various concentrations of xanthine and the XO inhibitors. Figure 8 shows the summary of the results of XO inhibition activity. AHPP inhibited XO in a competitive manner with an apparent inhibition constant Ki of 0.18 ± 0.02 μM, which was consistent with previous result (Fang et al. 2009a; Miyamoto et al. 1996). The apparent inhibitory constants (Ki) for mono-AHPP-PEG and bis-(AHPP)-PEG were estimated to be 0.23 ± 0.03 μM and 0.21 ± 0.03 μM, respectively. Both the AHPP conjugates show XO inhibition, which is comparable to native AHPP indicates AHPP-PEG conjugates itself is active towards XO. Similarly, PEGlylated AHPP conjugates may inhibit XO in a competitive manner.

In vivo pharmacokinetics of AHPP-PEG micelles

PEG-AHPP conjugates showed superior *in vivo* pharmacokinetics in ddY mice. The macromolecular micellar formulation of AHPP-PEG have relatively long circulation

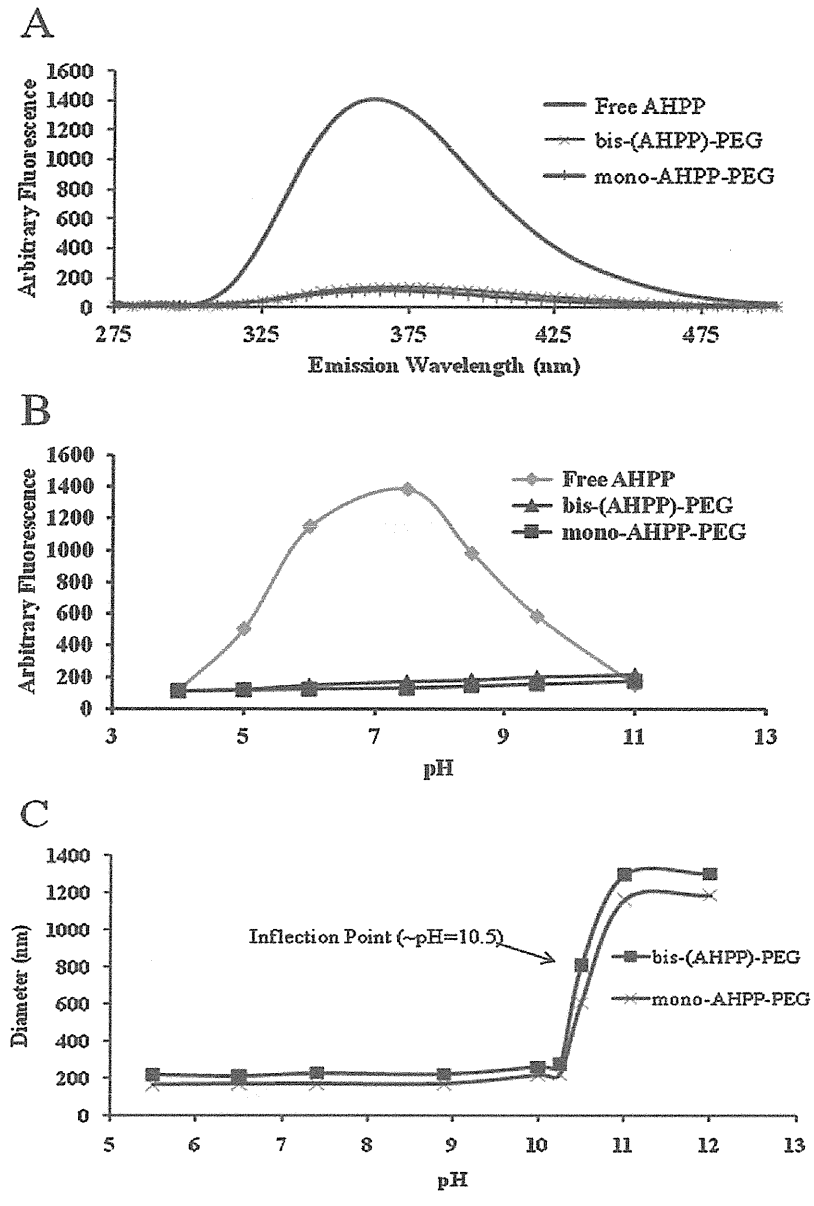

Figure 7. (A) Fluorescence spectra were recorded on F-2500 fluorospectrometer (Hitachi, Tokyo). The sample solutions were excited at 270.0 nm and emission from 275 to 500 nm was recorded, (B) The micellar stability of AHPP-PEG conjugates in different pH. The emission peak maxima (335.0 nm) were plotted against pH. (C) Micellar stability of conjugates (a) mono-AHPP-PEG and; (b) bis-(AHPP)-PEG was measured as a function of pH in various buffer solutions by DLS. Mostly micelles were nanoparticles (100–300 nm) in the range from pH 5.0 to pH 10.0 indicating their good stability in working pH range. Symbols: ■ mono-AHPP-PEG and ▲, bis-(AHPP)-PEG.

time: even 24 h after i.v. injection, about 35% remained in circulation, whereas more than 70% AHPP was cleared within 4 h after administration (Figure 9).

Discussion

In the present work, we synthesized PEG conjugated AHPP, which spontaneously formed micelles. Both conjugates showed potent XO inhibitory activity comparable to free AHPP and other polymer styrene-co-maleic acid copolymer (SMA) conjugated AHPP (Fang et al. 2009a). More importantly, the AHPP-PEG conjugates showed higher water solubility, which overcame the main drawback of native AHPP (which is practically water insoluble). The optimum AHPP content in the AHPP-PEG conjugates was about 7.5% for mono-AHPP-PEG and 15.1% for bis-(AHPP)-PEG, respectively.

Mean molecular weights of these conjugates of PEG-AHPP are about 2.2 and 2.3 kDa for mono-AHPP-PEG and bis-(AHPP)-PEG), respectively. However, Sephadex G-100 gel chromatography and DLS studies of AHPP-PEG conjugates indicated that they form supramolecular self-assembled association to form micellar structure in aqueous system; the critical micellar concentration

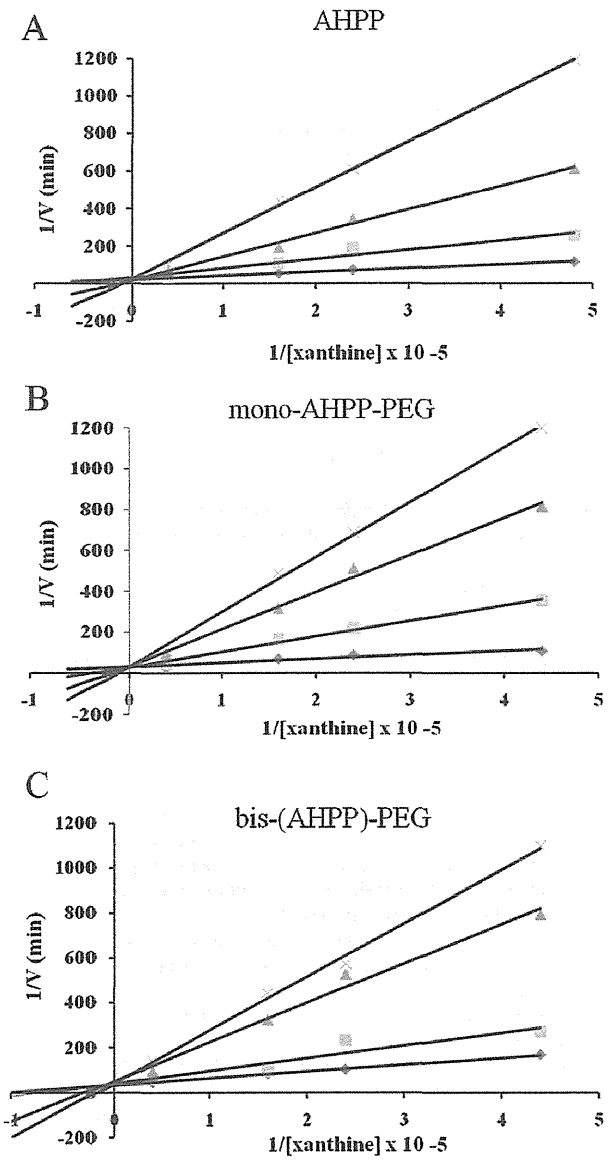

Figure 8. Lineweaver-Burk plot of PEG-AHPP conjugates for analysis of the XO inhibitory effects. (A) AHPP, (B) mono-AHPP-PEG and (C) bis-(AHPP)-PEG on the XO catalyze the oxidation of xanthine to uric acid. XO inhibitory activity of AHPP and AHPP-PEG conjugates was measured by measuring the rate of the uric acid formation in the presence of XO was determined spectrophotometrically. Concentrations and symbols for both conjugates used were: 0, ◆; 0.4, ■; 1.4, ▲; 2.4, and X, 4.4 μM. The apparent Ki values for AHPP, mono-AHPP-PEG and bis-(AHPP)-PEG were estimated to be 0.19 ± 0.03, 0.23 ± 0.03 μM and 0.21 ± 0.03 μM, respectively.

(CMC) of both AHPP-PEG conjugates was found to be about 0.3 mg/mL; therefore, above CMC level the AHPP-PEG conjugates will behave as macromolecule in blood circulation, thus exhibiting long plasma circulation time as evidenced by *in vivo* pharmacokinetics study (Figure 9). It is well known that biocompatible macromolecules show many beneficial characteristics such as prolonged

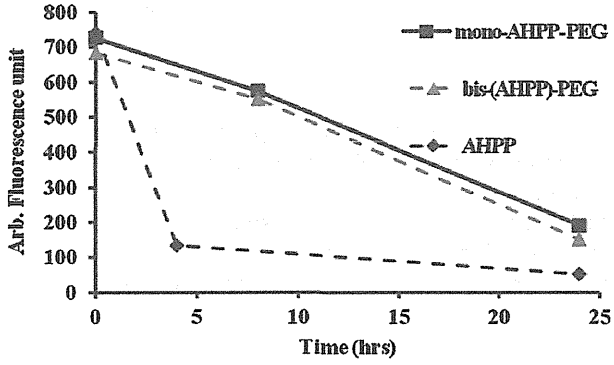

Figure 9. Pharmacokinetics of AHPP-PEG and native AHPP in blood of ddY mice. AHPP-PEG or native AHPP was injected i.v. into ddY mice via the tail vein. After scheduled intervals, mice were killed, blood was collected, and blood concentrations of AHPP and AHPP-PEG were measured as described in "methods". Values are means ± SE; $n = 3$.

in vivo half-life. For instance, the pyran copolymer-SOD derivatives synthesized in our laboratory showed prolonged plasma half-life of 6.0 h compared with ~4 min for the native SOD (Oda et al. 1989; Ogino et al. 1988). The result from this study (Figure 9) is in consistent to the previous reports. Furthermore, a PEGylated nanoscale polymeric carrier system provides stealth characteristics thereby prolonging plasma circulation time *in vivo* by avoiding uptake by reticuloendothelial system or phagocytic leukocytes (Sahoo et al. 2002; Greish et al. 2005).

The concept of macromolecular drugs is now widely applied in various clinical fields. For example, use of native interferon therapy has been almost replaced by PEG-interferon therapy (Iyer et al. 2006; Duncan et al. 2003; Vicent et al. 2006). PEG-ademase and PEG-aspargase are used for the severe combined immunodeficiency disease and leukemia respectively (Duncan et al. 2003). PEG is well accepted as safe drug carrier. Previously in our laboratory, pegylated anticancer agents like zinc protoporphyrin showed good tumor selectivity by taking advantage of EPR effect (Maeda et al. 2009a; Iyer et al. 2007a; Iyer et al. 2006). Thus, conjugates of AHPP-PEG not only resolves the problem of water-solubility, but it may take advantage of the pharmacokinetic merits because of its macromolecular micelle nature. Studies on cooperativity in the self-assembly of PEG-ZnPP, SMA-Pirarubicin, and SMA-ZnPP have been reported very recently (Sahoo et al. 2002; Iyer et al. 2007b; Greish et al. 2004; Fang et al. 2003). It was observed that AHPP-PEG micelles are more stable over the wide range of pH (5.0–10.0) probably because of strong interaction between AHPP head molecules, in the core of the micelles by forming hydrophobic associations.

The use of AHPP *in vivo* was first examined in spontaneous hypertensive rat (SHR model) for its antihypertensive effect (Miyamoto et al. 1996); wherein it was found that AHPP could reduced the blood pressure of SHR rat to ~70% of the initial blood pressure (Donald et al. 2009;

Miyamoto et al. 1996). It may thus be anticipated that the AHPP conjugated to PEG may improve the *in vivo* characteristics of the drug several folds, warranting further investigations.

Accordingly, from biological point of view, the principal objective of AHPP-PEG conjugation is to improve the pharmacokinetic drug profile. Along these lines AHPP-PEG conjugates may not only useful as an antihypertensive agent, but also may be beneficial for the treatment of ROS associated diseases such as heart diseases, prevention of $ONOO^-$ - mediated cytotoxicity and several others ROS related diseases. In addition, due to its macromolecular nature, AHPP-PEG conjugates may accumulate in the site of interest such as inflammation via the EPR effect (Maeda et al. 2001a), thus demonstrating its effect much selectively, whereas greatly decreases the potential side effects to the host.

In conclusion, we successfully synthesized AHPP-PEG conjugates by utilizing two different approaches. AHPP-PEG derivatives exhibit much improved water solubility and superior *in vivo* pharmacokinetics as well as potent XO inhibiting activity. As XO is the major cause of O_2^- in many diseases, we thus anticipate the application of AHPP-PEG conjugates for the treatment of ROS related diseases, which warrants further investigations.

Acknowledgments

We would like to acknowledge Prof. Toshihiro Nohara, Laboratory of Natural Medicine, Department of Pharmaceutical Sciences, Sojo University for discussion and suggestions regarding characterization.

Declaration of interest

This work was supported by Grants-in-Aid for Scientific Research on Cancer Priority Areas (20015045), Scientific Research (C) (20590049) and (S0801085) from the Ministry of Education, Culture, Sports, Science and Technology of Japan, and a grant from the Ministry of Health, Welfare and Labour (No. 23000001, H 23-3) 3rd Cancer Study Project of Japan, to H.M. Bharate G. Y. would like to thank Sojo University and BioDynamics Research Foundation, Japan, for a Fellowship to PhD studies. The authors declare no conflicts of interest.

References

Adachi T, Fukushima T, Usami Y, Hirano K. (1993). Binding of human xanthine oxidase to sulphated glycosaminoglycans on the endothelial-cell surface. Biochem J, 289 (Pt 2), 523–527.

Cappola TP, Kass DA, Nelson GS, Berger RD, Rosas GO, Kobeissi ZA, Marbán E, Hare JM. (2001). Allopurinol improves myocardial efficiency in patients with idiopathic dilated cardiomyopathy. Circulation, 104, 2407–2411.

Crow JP, Beckman JS. (1995). The role of peroxynitrite in nitric oxide-mediated toxicity. In: Koprowski H, Maeda H. (eds.). The Role of Nitric Oxide in Physiology and Pathophysiology. Current Topics in Microbiology and Immunology. Springer-Verlag, Berlin 196:57–73.

Donald LJ, Robert A, Mercedes C, Giovanni DS, Ferguson TB, Flegal K, Ford E, Furie K, Alan G, Greenlund K, Haase N, Hailpern S, Michael H, Howard V, Kissela B, Kittner S, Lackland D, Lisabet, L, Marelli A, McDermott M, Meigs J, Mozaffarian D, Nichol G, O'Donnell C, Roger V, Rosamond W, Sacco R, Sorlie P, Stafford R, Steinberger J, Thom T, Wasserthiel-Smoller S, Wong N, Wylie-Rosett J, Hong Y. (2009). Heart Disease and Stroke Statistics_2009. Update: A Report From the American Heart Association Statistics Committee and Stroke Statistics Subcommittee. Circulation 119:e21–e181.

Duncan R. (2003). The dawning era of polymer therapeutics. Nat Rev Drug Discov, 2, 347–360.

Fang J, Sawa T, Akaike T, Akuta T, Sahoo SK, Khaled G, Hamada A, Maeda H. (2003). *In vivo* antitumor activity of pegylated zinc protoporphyrin: targeted inhibition of heme oxygenase in solid tumor. Cancer Res, 63, 3567–3574.

Fang J, Iyer AK, Seki T, Nakamura H, Greish K, Maeda H. (2009a). SMA-copolymer conjugate of AHPP: a polymeric inhibitor of xanthine oxidase with potential antihypertensive effect. J Control Release, 135, 211–217.

Fang J, Seki T, Maeda H. (2009b). Therapeutic strategies by modulating oxygen stress in cancer and inflammation. Adv Drug Deliv Rev, 61, 290–302.

Feigelson P, Davidson JD, Robins RK. (1957). Pyrazolopyrimidines as inhibitors and substrates of xanthine oxidase. J Biol Chem, 226, 993–1000.

Freehold NJ. (1972). Xanthine Oxidase (milk). In: Worthington Enzyme Manual. Worthington Biochemical, pp. 30–31.

Greish K, Sawa T, Fang J, Akaike T, Maeda H. (2004). SMA-doxorubicin, a new polymeric micellar drug for effective targeting to solid tumours. J Control Release, 97, 219–230.

Greish K, Nagamitsu A, Fang J, Maeda H. (2005). Copoly(styrene-maleic acid)-pirarubicin micelles: high tumor-targeting efficiency with little toxicity. Bioconjug Chem, 16, 230–236.

Gryglewski RJ, Palmer RM, Moncada S. (1986). Superoxide anion is involved in the breakdown of endothelium-derived vascular relaxing factor. Nature, 320, 454–456.

Harada A, Kataoka K. (1999). Chain length recognition: core-shell supramolecular assembly from oppositely charged block copolymers. Science, 283, 65–67.

Huie RE, Padmaja S. (1993). The reaction of NO with superoxide. Free Radic Res Commun, 18, 195–199.

Ideta R, Tasaka F, Jang WD, Nishiyama N, Zhang GD, Harada A, Yanagi Y, Tamaki Y, Aida T, Kataoka K. (2005). Nanotechnology-based photodynamic therapy for neovascular disease using a supramolecular nanocarrier loaded with a dendritic photosensitizer. Nano Lett, 5, 2426–2431.

Iyer AK, Khaled G, Fang J, Maeda H. (2006). Exploiting the enhanced permeability and retention effect for tumor targeting. Drug Discov Today, 11, 812–818.

Iyer AK, Greish K, Seki T, Okazaki S, Fang J, Takeshita K, Maeda H. (2007a). Polymeric micelles of zinc protoporphyrin for tumor targeted delivery based on EPR effect and singlet oxygen generation. J Drug Target, 15, 496–506.

Iyer AK, Greish K, Fang J, Murakami R, Maeda H. (2007b). High-loading nanosized micelles of copoly(styrene-maleic acid)-zinc protoporphyrin for targeted delivery of a potent heme oxygenase inhibitor. Biomaterials, 28, 1871–1881.

Jarasch ED, Bruder G, Heid HW. (1986). Significance of xanthine oxidase in capillary endothelial cells. Acta Physiol Scand Suppl, 548, 39–46.

Jarasch ED, Grund C, Bruder G, Heid HW, Keenan TW, Franke WW. (1981). Localization of xanthine oxidase in mammary-gland epithelium and capillary endothelium. Cell, 25, 67–82.

Maeda H. (2001a). SMANCS and polymer-conjugated macromolecular drugs: advantages in cancer chemotherapy. Adv Drug Deliv Rev, 46, 169–185.

Maeda H. (2001b). The enhanced permeability and retention (EPR) effect in tumor vasculature: the key role of tumor-selective macromolecular drug targeting. Adv Enzyme Regul, 41, 189–207.

Maeda H, Sawa T, Konno T. (2001c). Mechanism of tumor-targeted delivery of macromolecular drugs, including the EPR effect in solid tumor and clinical overview of the prototype polymeric drug SMANCS. J Control Release, 74, 47–61.

Maeda H. (2009a). Controlling oxidative stress: therapeutic and delivery strategies. Preface. Adv Drug Deliv Rev, 61, 285–286.

Maeda H, Bharate GY, Daruwalla J. (2009b). Polymeric drugs for efficient tumor-targeted drug delivery based on EPR-effect. Eur J Pharm Biopharm, 71, 409–419.

Matsumura Y, Maeda H. (1986). A new concept for macromolecular therapeutics in cancer chemotherapy: mechanism of tumoritropic accumulation of proteins and the antitumor agent smancs. Cancer Res, 46, 6387–6392.

Miyamoto Y, Akaike T, Yoshida M, Goto S, Horie H, Maeda H. (1996). Potentiation of nitric oxide-mediated vasorelaxation by xanthine oxidase inhibitors. Proc Soc Exp Biol Med, 211, 366–373.

Moncada S, Palmer RM, Higgs EA. (1991). Nitric oxide: physiology, pathophysiology, and pharmacology. Pharmacol Rev, 43, 109–142.

Nishide H, Mihayashi K, Tsuchida E. (1977). Dissociation of aggregated ferroheme complexes and protoporphyrin IX by water-soluble polymers. Biochim Biophys Acta, 498, 208–214.

Oates JA, Brown NJ. (2001). Antihypertensive agents and the drug therapy of hypertension. In: Hardman JG, Limbird LE, Gilman AG, (eds.).Goodman & Gilman's the pharmacological basis of therapeutics (10th Edition), The McGraw-Hill Companies, Inc., New York. pp. 871–896.

Oda T, Akaike T, Hamamoto T, Suzuki F, Hirano T, Maeda H. (1989). Oxygen radicals in influenza-induced pathogenesis and treatment with pyran polymer-conjugated SOD. Science, 244, 974–976.

Ogino T, Inoue M, Ando Y, Awai M, Maeda H, Morino Y. (1988). Chemical modification of superoxide dismutase. Extension of plasma half life of the enzyme through its reversible binding to the circulating albumin. Int J Pept Protein Res, 32, 153–159.

Otsuka H, Nagasaki Y, Kataoka K. (2003). PEGylated nanoparticles for biological and pharmaceutical applications. Adv Drug Deliv Rev, 55, 403–419.

Pacher P, Nivorozhkin A, Szabó C. (2006). Therapeutic effects of xanthine oxidase inhibitors: renaissance half a century after the discovery of allopurinol. Pharmacol Rev, 58, 87–114.

Radi R, Beckman JS, Bush KM, Freeman BA. (1991). Peroxynitrite oxidation of sulfhydryls. The cytotoxic potential of superoxide and nitric oxide. J Biol Chem, 266, 4244–4250.

Sahoo SK, Sawa T, Fang J, Tanaka S, Miyamoto Y, Akaike T, Maeda H. (2002). Pegylated zinc protoporphyrin: a water-soluble heme oxygenase inhibitor with tumor-targeting capacity. Bioconjug Chem, 13, 1031–1038.

Stocks SJ, Jones AJ, Ramey CW, Brooks DE. (1986). A fluorometric assay of the degree of modification of protein primary amines with polyethylene glycol. Anal Biochem, 154, 232–234.

Veronese FM, Largajolli R, Boccù E, Benassi CA, Schiavon O. (1985). Surface modification of proteins. Activation of monomethoxy-polyethylene glycols by phenylchloroformates and modification of ribonuclease and superoxide dismutase. Appl Biochem Biotechnol, 11, 141–152.

Veronese FM, Schiavon O, Pasut G, Mendichi R, Andersson L, Tsirk A, Ford J, Wu G, Kneller S, Davies J, Duncan R. (2005). PEG-doxorubicin conjugates: influence of polymer structure on drug release, *in vitro* cytotoxicity, biodistribution, and antitumor activity. Bioconjug Chem, 16, 775–784.

Vicent MJ, Duncan R. (2006). Polymer conjugates: nanosized medicines for treating cancer. Trends Biotechnol, 24, 39–47.

International Journal of Pharmaceutics 420 (2011) 111–117

Contents lists available at ScienceDirect

International Journal of Pharmaceutics

journal homepage: www.elsevier.com/locate/ijpharm

Pharmaceutical Nanotechnology

Synthesis and evaluation of poly(styrene-*co*-maleic acid) micellar nanocarriers for the delivery of tanespimycin

Nate Larson[a,b], Khaled Greish[a,b,*,1], Hillevi Bauer[a,b], Hiroshi Maeda[d], Hamidreza Ghandehari[a,b,c,**]

[a] *Department of Pharmaceutics and Pharmaceutical Chemistry, Salt Lake City, UT 84108, USA*
[b] *Center for Nanomedicine, Nano Institute of Utah, Salt Lake City, UT 84108, USA*
[c] *Department of Bioengineering, University of Utah, Salt Lake City, UT 84108, USA*
[d] *Research Institution of DDS, Sojo University, Kumamoto 860-0082, Japan*

ARTICLE INFO

Article history:
Received 9 May 2011
Received in revised form 28 July 2011
Accepted 8 August 2011
Available online 12 August 2011

Keywords:
Tanespimycin
17-AAG
Polymeric micelle
Prostate cancer

ABSTRACT

Polymeric micelles carrying the heat shock protein 90 inhibitor tanespimycin (17-*N*-allylamino-17-demethoxygeldanamycin) were synthesized using poly(styrene-*co*-maleic acid) (SMA) copolymers and evaluated *in vitro* and *in vivo*. SMA-tanespimycin micelles were prepared with a loading efficiency of 93%. The micelles incorporated 25.6% tanespimycin by weight, exhibited a mean diameter of 74 ± 7 nm by dynamic light scattering and a zeta potential of −35 ± 3 mV. Tanespimycin was released from the micelles in a controlled manner *in vitro*, with 62% released in 24 h from a pH 7.4 buffer containing bovine serum albumin. The micellar drug delivery systems for tanespimycin showed potent activity against DU145 human prostate cancer cells, with an IC_{50} of 230 nM. They further exhibited potent anti-cancer activity *in vivo* in nu/nu mice bearing subcutaneous DU145 human prostate cancer tumor xenografts, with significantly higher anticancer efficacy as measured by tumor regression when compared to free tanespimycin at an equivalent single dose of 10 mg/kg. These data suggest further investigation of SMA-tanespimycin as a promising agent in the treatment of prostate cancer.

1. Introduction

Heat shock protein 90 (Hsp90) is a 90 kDa chaperone protein that facilitates the cellular response to stress by regulating the folding and activity of many client proteins, which include critical growth-stimulating proteins involved in the malignant transformation of various cancers (Sharp and Workman, 2006). Hsp90 expression is elevated during cellular stress conditions such as heat, pH, and glucose deprivation (Buchner, 1999) and in a variety of cancers including melanoma, leukemia, colon, lung, breast, and prostate (Fukuyo et al., 2010).

Geldanamycin (GDM), a benzoquinone ansamycin derived from *Streptomyces hygrocopicus*, is a naturally occurring inhibitor of Hsp90 and has been studied extensively as an anticancer agent (Porter et al., 2009). GDM binds to the N-terminal ATP-binding site of Hsp90 and induces degradation of its client proteins (Whitesell and Lindquist, 2005). This ability of GDM to alter multiple oncogenic pathways makes GDM an attractive therapeutic compound. However, the clinical use of GDM has been limited by multiple factors. It exhibits high hepatotoxicity at therapeutic doses in animal models (Supko et al., 1994), is poorly soluble in water, and is metabolically unstable (Fukuyo et al., 2010). A GDM derivative 17-*N*-allylamino-17-demethoxygeldanamycin (tanespimycin, 17-AAG) has been widely investigated as an alternative to GDM, and has shown less toxicity and comparable activity compared to GDM in mouse models (Kelland et al., 1999; Burger et al., 2004). This drug was the first-in-class Hsp90 inhibitor to enter clinical trials (Banerji et al., 2005). Although the therapeutic index for tanespimycin is increased as compared to GDM, dose limiting toxicity is still due to hepatic and gastrointestinal symptoms (Sausville et al., 2003). Delivery of tanespimycin is difficult due a poor aqueous solubility of 0.02–0.05 mg/mL (Ge et al., 2006), requiring the use of surfactants such as Cremophor® EL, which are known to induce histamine release, resulting in hypersensitivity reactions and anaphylaxis (Rowinsky and Donehower, 1995), and are further associated with hyperlipidaemia, abnormal lipoprotein patters, aggregation of erythrocytes, and peripheral neuropathy (Gelderblom et al., 2001).

* Corresponding author at: Department of Pharmaceutics and Pharmaceutical Chemistry, University of Utah, 383 Colorow Road, Room 339, Salt Lake City, UT 84108, USA. Tel.: +1 801 587 1558.
** Corresponding author at: Department of Pharmaceutics and Pharmaceutical Chemistry and Bioengineering, University of Utah, 383 Colorow Road, Room 343, Salt Lake City, UT 84108, USA. Tel.: +1 801 587 1566.
E-mail addresses: khaled.gerish@utah.edu, khaled.gerish@otago.ac.nz (K. Greish), hamid.ghandehari@pharm.utah.edu (H. Ghandehari).
[1] *Present address*: Department of Pharmacology & Toxicology, Otago School of Medical Sciences, University of Otago, Dunedin, New Zealand, Tel.: + 64 3 479 4095; + 64 21 310 335.

0378-5173/$ – see front matter © 2011 Elsevier B.V. All rights reserved.
doi:10.1016/j.ijpharm.2011.08.011

Polymeric carriers can increase the solubility of poorly water soluble drugs and can accumulate in tumor tissues via the "enhanced permeability and retention" (EPR) effect (Matsumura et al., 1987; Greish et al., 2003), thereby increasing the therapeutic index for a given chemotherapeutic agent. Polymeric micelles are characterized by a hydrophilic shell which interacts with an external aqueous environment and a hydrophobic core which acts as a depot for hydrophobic drugs. Polymeric micelles were first reported as potential carriers for use in cancer treatment in the early 1980s (Gros et al., 1981) and the field has matured to include a number of candidates currently under clinical investigation (Blanco et al., 2009).

The use of poly(styrene-*co*-maleic acid) (SMA) micelles as drug carriers is currently under investigation (Iyer et al., 2007; Daruwalla et al., 2010). SMA has been proven to be biologically safe and is used clinically in SMANCS, a conjugate of half-butyl SMA bound to the antitumor protein neocarzinostatin (Maeda, 2001). Previous studies have demonstrated immunopotentiating activity associated with SMA moieties, in contrast to immunosuppression that is typically induced by conventional chemotherapeutics (Suzuki et al., 1988, 1990). The styrenic core of SMA micelles has been characterized by a high glass transition temperature (Rodriguez et al., 2008) and a large microviscosity (Claracq et al., 2002), which may help facilitate higher stability and more controlled release rates of drugs from the micelle core. In addition, the hydrophilic surface of SMA micelles is comprised of carboxyl terminated maleic acid groups, allowing easy surface modification or conjugation with targeting moieties.

Previous work by our group (Borgman et al., 2009; Larson et al., 2010) and others (Kasuya et al., 2002) has described the use of HPMA copolymers as drug carriers for geldanamycin derivatives. In these systems, geldanamycin derivatives are covalently bound to the polymer backbone via the lysosomally degradable Gly-Phe-Leu-Gly linker (Subr et al., 1988), resulting in highly stable conjugates with drug release occurring via lysosomal degradation following endocytosis. The use of such systems however requires chemical modification of geldanamycin to facilitate conjugation, and such modifications result in a decrease in the activity of geldanamycin. Self-assembled drug delivery systems do not suffer from this limitation as the drug is most often bound to the carrier through non-covalent hydrophobic interactions.

In the present study, SMA was used to prepare polymeric micelles containing the Hsp90 inhibitor tanespimycin. The micelles were characterized for drug loading efficiency, drug content, size, and zeta potential. The release rate of tanespimycin from the micelles and the ability of the micelles to inhibit the growth of DU145 human prostate cancer cells *in vitro* were evaluated. An *in vivo* preliminary single dose study evaluating the efficacy of the micelles was performed in nu/nu mice bearing DU145 human prostate cancer xenografts.

2. Materials and methods

2.1. Materials

Geldanamycin (NSC 122750) was kindly supplied by the National Cancer Institute Developmental Therapeutics Program (NCI DTP). Allylamine was supplied by Alfa Aesar (Ward Hill, MA, USA). Cumene terminated poly(styrene-*co*-maleic anhydride) was obtained from Sigma–Aldrich Corp. (St. Louis, MO, USA) and supplied with a 1.3:1 mole ratio of styrene:maleic anhydride, an average M_n of approximately 1600 as determined by GPC, and an acid number of 465–495 mg KOH/g. *N*-(3-Dimethylaminopropyl)-*N*′-ethylcarbodiimide hydrochloride (EDAC) was obtained from Sigma–Aldrich Corp. Bovine serum albumin (BSA) fraction V was obtained from MP Biomedicals (Solon, OH, USA). Polyoxyl castor oil (Cremophor® EL) was obtained from BASF Corp. (Florham Park, NJ, USA). Poly(ethylene glycol) 400 was obtained from Dow Chemical Corp. (Petaluma, CA, USA).

2.2. Cell lines and culture

The human prostate cancer cell line DU145 (ATCC, Rockville, MD, USA) was maintained in Eagle's minimum essential medium (ATCC) supplemented with 10% heat inactivated fetal bovine serum. Cell lines were cultured at 37 °C in a humidified atmosphere of 5% CO_2. For all procedures, cells were harvested using TrypLE™ Express (Invitrogen, Carlsbad, CA) and cell lines were maintained in a logarithmic growth phase during all studies.

2.3. Synthesis of tanespimycin

200 mg (0.357 mmol) of GDM was dissolved in 10 mL anhydrous dimethylformamide (DMF) at ambient temperature. 80.1 μL (1.07 mmol) of allylamine was added and the solution was kept under nitrogen, protected from exposure to light, and allowed to stir overnight at ambient temperature. The color of the solution changed from bright yellow-orange to dark purple and completion of the reaction was monitored by TLC on silica gel with chloroform:MeOH [9:1] as mobile phase by the disappearance of GDM. DMF was removed by rotary evaporator, and the resulting crude product was recrystallized from H_2O:EtOH [4:1]. The precipitate was analyzed by electrospray ionization mass spectrometry (ESI-MS).

2.4. Preparation of SMA-tanespimycin

Preparation of SMA micelles was similar to the method previously reported with modifications (Greish et al., 2004). First, poly(styrene-*co*-maleic anhydride) was hydrolyzed under aqueous alkaline conditions. Deionized water was adjusted to pH 14 with 4 N NaOH and heated to 70 °C. Poly(styrene-*co*-maleic anhydride) was added under stirring and the solution was maintained at pH 14 and 70 °C. The resulting hydrolyzed SMA solution was adjusted to pH 7.0 with 1 N HCl, diluted to a final concentration of 50 mg/mL, and allowed to cool to ambient temperature. 12 mL (600 mg SMA) was removed and diluted to approximately 60 mL with deionized water. 200 mg of tanespimycin was dissolved in minimal DMSO, and added drop wise while stirring, resulting in a cloudy solution. The solution was then adjusted to a pH of 5.0 and 600 mg EDAC in 5 mL deionized water was added drop wise at pH 5.0 and allowed to stir for 30 min. Next, the solution was adjusted to pH 10.5 by the addition of 1 N NaOH, the pH was subsequently adjusted to 7.0 with 1 N HCl, and the resulting solution was filtered to remove undissolved tanespimycin. 1 N HCl was then added dropwise to the filtrate to precipitate the micelles. The precipitated micelles were then centrifuged and purified by washing repeatedly with cold 0.01 N HCl in deionized water. Residual water/HCl was removed by lyophilization to obtain the final SMA-tanespimycin product.

2.5. Loading efficiency of SMA-tanespimycin

For the purpose of this study, loading efficiency is defined as the total weight of the drug in the final SMA-tanespimycin product divided by the initial weight of the drug introduced for micellar preparation. A standard curve was prepared by serial dilution of tanespimycin in DMSO and quantification of the drug was by UV spectrometry at 335 nm. Loading efficiency and drug content were then obtained by dissolving SMA-tanespimycin in DMSO and measuring absorbance at 335 nm in comparison with the standard curve.

To ensure that the drug was unmodified during micelle preparation, SMA-tanespimycin was further analyzed by reversed phase high-performance liquid chromatography (RP-HPLC). Analysis was performed with an Agilent 1100 LC system equipped with an Alltech Alltima C18 5 μm 150 × 4.6 mm column and a photo diode array detector scanning at 200–500 nm. The mobile phase consisted of deionized water and acetonitrile (ACN), at the following gradient: analysis time 0 min, 35% ACN; 15 min, 65% ACN; 25 min, 75% ACN; 30 min 95% ACN; 39 min, 100% ACN; 40 min, 65% ACN. A post time of 5 min was used to allow column equilibration between samples. The flow rate was maintained at 1.0 mL/min throughout and the sample injection volume was 20 μL. Samples of tanespimycin and SMA-tanespimycin were prepared in deionized water:ACN [65:35] and injected for analysis. The λ_{max} of tanespimycin at 335 nm was used for final quantitative analysis.

2.6. Size and zeta potential of SMA-tanespimycin

SMA-tanespimycin was prepared in 50 mM sodium phosphate buffer pH 7.4 at a concentration of 1.0 mg/mL for analysis. All measurements were performed at 25 °C. A Malvern Zeta Sizer ZEN3600 (Malvern Instruments Inc., Westborough, MA) was used to determine mean *Z*-average size, size distribution and zeta-potential. All measurements were performed on three separately prepared samples.

2.7. Drug release from SMA-tanespimycin

The release of tanespimycin from the micellar preparations was evaluated using a dialysis method and compared to the release in a standard vehicle formulation of EtOH:Cremophor® EL:PEG 400 [2:1:1] (EtOH:CrEL:PEG) (Zhong and Licari, 2005). SMA-tanespimycin was prepared at a concentration of 2.5 mg/mL (0.625 mg/mL tanespimycin) and drug-EtOH:CrEL:PEG was prepared by dissolving tanespimycin in EtOH:CrEL:PEG followed by a 10× dilution to yield a final concentration of 0.625 mg/mL. Samples were prepared in a 50 mM sodium phosphate buffer pH 7.4 or phosphate buffered saline (PBS) pH 7.4 with 40 mg/mL BSA. 4 mL of each sample was placed in a dialysis tube with a molecular weight cutoff of 3500 Da and dialyzed against 5 L of either 50 mM sodium phosphate buffer pH 7.4 or PBS pH 7.4. Media outside the dialysis membrane was changed periodically to ensure a constant sink condition. At each predetermined time point, 200 μL of the sample inside the dialysis membrane was removed and analyzed spectrophotometrically at 335 nm. Quantification of percent release was performed by comparison of sample absorbance with calibration curves prepared for SMA-tanespimycin and tanespimycin-EtOH-CrEL:PEG for each test condition. All experiments were performed in triplicate. Percent release is reported as mean ± standard deviation.

2.8. In vitro growth inhibition against human prostate cancer cells

The ability of the SMA-tanespimycin to inhibit the growth of DU145 human prostate cancer cells was evaluated using a 2-(2-methoxy-4-nitrophenyl)-3-(4-nitrophenyl)-5-(2,4-disulfophenyl)-2H-tetrazolium,monosodium salt (WST-8) cell viability assay. 3000 DU145 cells per well were plated in 96-well plates for 24 h. Cell culture medium was then removed and cells were treated with SMA-tanespimycin, tanespimycin dissolved in EtOH:CrEL:PEG, or controls for 72 h. Following treatment, medium was removed and wells were washed with 200 μL PBS. 100 μL of 10% (v/v) WST-8 reagent in complete growth medium was added to each well, cells were incubated at 37 °C/5% CO_2 for 120 min and absorbance at 450 nm minus 630 nm was determined by UV spectrophotometry. Relative viability was calculated by normalization of the absorbance of untreated cells. All experiments were performed in triplicate, with $n = 3$ wells per replicate. Non-linear least-squares regression analysis and calculation of IC_{50} was performed using GraphPad Prism.

2.9. In vivo efficacy

Six-week-old athymic (*nu/nu*) mice were obtained from Charles River Laboratories (Davis, CA, USA) and used in accordance with the Institutional Animal Care and Use Committee (IACUC) of the University of Utah. Mice were anesthetized using 4% isoflurane mixed with oxygen followed by subcutaneous injection of 1×10^7 DU145 cells per flank ($n = 5$ mice per treatment group). When the mean tumor size had reached approximately 50 mm^3 (about 10 days after tumor inoculation), the mice were treated with a single injection of either saline (control), free tanespimycin dissolved in DMSO, or SMA-tanespimycin at a dose of 10 mg/kg drug equivalent. The animals were routinely monitored and tumor growth was measured twice weekly and tumor volume was calculated as length × width^2 × $\pi/6$. Tumor volumes at each time point were normalized by the initial tumor volume and are reported as mean ± standard error of the mean. Animal weights were also measured at each time point and normalized to initial weight reported as mean ± standard deviation.

2.10. Statistical analysis

For release studies, tumor regression, and animal weight data, differences between data sets were determined by two-way repeated measures ANOVA using GraphPad Prism. Where differences were detected, a Bonferroni post-test was used to test for significance between groups. The significance level was set to $\alpha = 0.05$ for all statistical tests.

3. Results and discussion

3.1. Synthesis and preparation of SMA-tanespimycin

The development of polymeric micelles in drug delivery has primarily focused on the use of amphiphilic block copolymers with poly(ethylene glycol) (PEG) as the hydrophilic segment and a polyester or a poly(amino acid) derivative as the hydrophobic segment (Croy and Kwon, 2006). The loading of hydrophobic drugs and the assembly of such copolymers into micellar structures is commonly performed using methods such as: (1) basic equilibration, (2) dialysis, (3) oil/water emulsion, (4) solution casting, or (5) freeze drying (Gaucher et al., 2005). The present study describes polymeric micelles prepared by varying the pH of an aqueous solution containing poly(styrene-*co*-maleic acid) copolymers and tanespimycin, as a hydrophobic drug.

Tanespimycin was synthesized from GDM, and the resulting purple solid was collected and identified as tanespimycin by ESI-MS. SMA-tanespimycin was prepared by varying the pH of an aqueous solution of hydrolyzed SMA (Fig. 1).

3.2. Characterization of SMA-tanespimycin

The preparation of polymeric micelles as drug carriers often employ methods that result in either low loading efficiency or low drug loading capacity (Park, 2007). Using the aforementioned process, hydrolyzed SMA incorporated tanespimycin with a loading efficiency of 93% (Table 1), a significant improvement over previous studies describing polymeric micellar formulations of tanespimycin (Xiong et al., 2009; Shin et al., 2009).

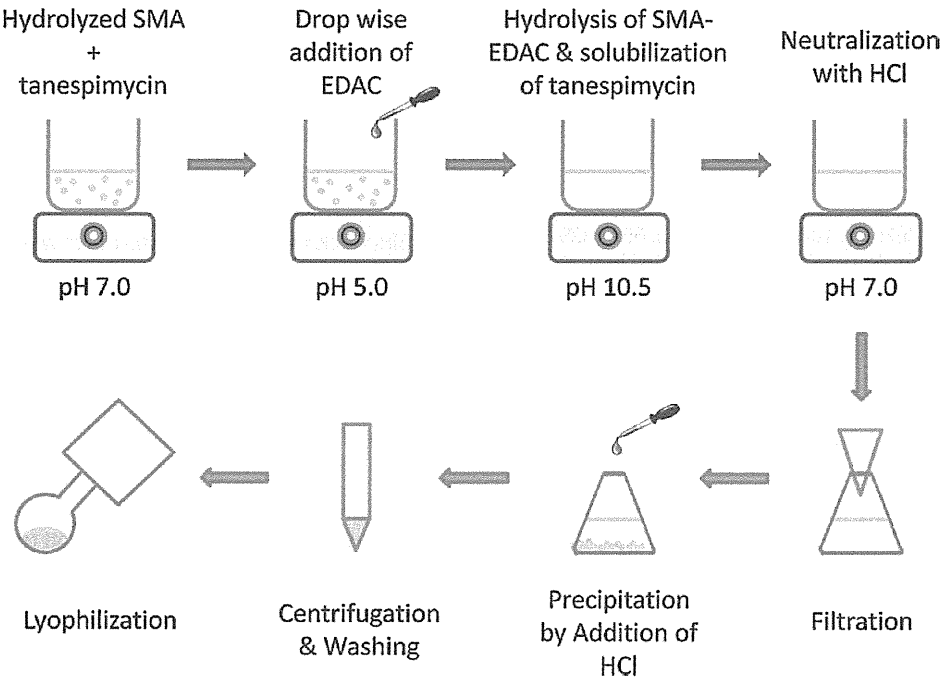

Fig. 1. Preparation of SMA-tanespimycin micelles. SMA-tanespimycin micelles were prepared by first suspending tanespimycin in an aqueous solution of hydrolyzed SMA containing EDAC. The solution was then adjusted to alkaline conditions which resulted in encapsulation of tanespimycin by SMA micelles. The resulting solution was neutralized and SMA-tanespimycin micelles isolated.

The ability of SMA based micelles to achieve high drug loading has previously been demonstrated for the hydrophobic drugs zinc protoporphyrin (Iyer et al., 2007) and doxorubicin (Greish et al., 2004). In the current study, a high drug loading of 25.6% tanespimycin by weight was observed for SMA-tanespimycin as determined by UV spectrophotometry (Table 1). The micelles were highly soluble, with a drug equivalent aqueous solubility of >5.0 mg/mL as measured in pH 7.4 PBS buffer, whereas free tanespimycin was soluble only at 0.021 mg/mL. To ensure that tanespimycin remained unmodified during micelle preparation, SMA-tanespimycin in comparison with free tanespimycin was analyzed by RP-HPLC. Both tanespimycin and SMA-tanespimycin showed a prominent peak at 15.2 min, and both peaks exhibited UV spectra characteristic of tanespimycin (data not shown). Drug loading of tanespimycin as determined by RP-HPLC was 25.2% by weight and in agreement with drug loading determined by UV spectrophotometry.

Size is a critical parameter for macromolecular drug delivery systems designed to escape renal filtration. It has been proposed that carriers with sizes greater than 10 nm accumulate in the tumor tissues via the EPR effect. SMA-tanespimycin micelles had a mean diameter of 74 ± 7 nm and a polydispersity index of 0.31 ± 0.08 as measured by dynamic light scattering (Fig. 2). The micelles had a zeta potential of -35 ± 3 mV as measured in a 50 mM phosphate buffer at pH 7.4. SMA micelles were characterized by carboxyl terminated maleic acid surface groups which impart a negative charge to the micelles.

The high loading efficiency and possibility to tune the loading ratio of tanespimycin into SMA micelles represents significant advantages for industrial scale up, in contrast to many other micellar systems.

Table 1
Characteristics of SMA-tanespimycin micelles.

Property	Mean	SD
Amount of tanespimycin introduced for micelle preparation (mg)	150.0	–
Drug loading efficiency (%)[a]	93.1	–
Drug loading (% wt/wt)	25.6	–
Mean micelle diameter (nm)[b,c]	74	7
Polydispersity index	0.31	0.08
Zeta potential[c](mV)	−35	3

[a] Drug loading efficiency calculated as mg tanespimycin solubilized by SMA micelles/mg tanespimycin introduced for micelle preparation.
[b] Z-Average size as measured by dynamic light scattering (DLS).
[c] As measured in 50 mM phosphate buffer at pH 7.4.

3.3. Release of tanespimycin from SMA-tanespimycin micelles

The incorporation of tanespimycin into SMA micelles can increase tumor uptake and alter biodistribution, resulting in an increase in the therapeutic index of the drug. For this to occur, it is essential that tanespimycin is retained by the carrier for a period of time to allow drug accumulation in tumor tissue via

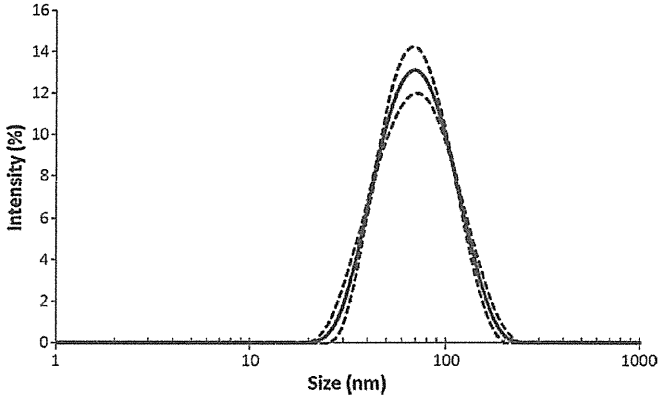

Fig. 2. Size distribution of SMA-tanespimycin micelles. The size distribution of SMA-tanespimycin micelles was determined using a Malvern Zeta Sizer at a concentration of 1.0 mg/mL at pH 7.4. Data are expressed as mean (solid line) ± SD (dashed line) ($N = 3$).

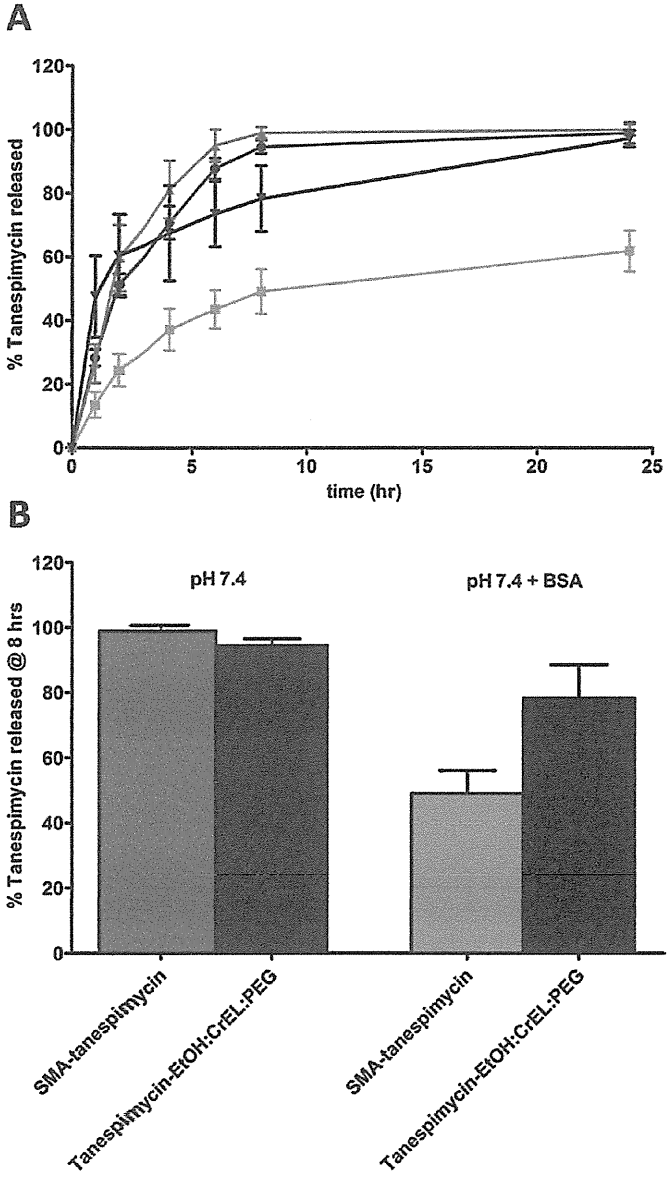

Fig. 3. Release of tanespimycin from SMA-tanespimycin. Release of tanespimycin from SMA micelles was evaluated using a dialysis method and compared to tanespimycin formulated in EtOH:CrEL:PEG as control. (A) Release of tanespimycin from SMA-tanespimycin (red) and tanespimycin-EtOH:CrEL:PEG (blue) in a pH 7.4 buffer and release of tanespimycin from SMA-tanespimycin (green) and tanespimycin-EtOH:CrEL:PEG (black) in a pH 7.4 buffer containing 40 mg/mL BSA. (B) Release of tanespimycin at 8 h. Data expressed as mean ± SD ($N = 3$). *Difference detected at $p < 0.05$ significance level. (For interpretation of the references to color in the figure caption, the reader is referred to the web version of the article.)

the EPR effect. However, release from the carrier is also essential to allow tanespimycin to elicit its pharmacologic effect. Release rate is therefore a critical parameter in anticancer macromolecular drug delivery, and an ideal anticancer carrier should be able to retain its cargo for approximately 6 h while tumor accumulation occurs (Greish, 2007), followed by complete drug release. To address this issue, the *in vitro* release rate of tanespimycin from SMA-tanespimycin micelles was evaluated using a dialysis method and compared to the release of tanespimycin formulated in EtOH:CrEL:PEG. Release was assessed in a pH 7.4 buffer where 51% and 95% tanespimycin was released from SMA-tanespimycin micelles in 2 and 8 h, respectively. Release from tanespimycin formulated in EtOH:CrEL:PEG was not significantly different, with 60% and 99% released in 2 and 8 h, respectively. To better ascertain release of tanespimycin from the blood plasma compartment *in vivo*, a second test condition was evaluated wherein BSA was included inside the dialysis bag at a physiologically relevant concentration of 40 mg/mL. Release of tanespimycin from SMA-tanespimycin micelles in the presence of BSA was reduced at all time points greater that 1 h ($p < 0.001$) as compared to release from pH 7.4 buffer alone (Fig. 3). Release of tanespimycin from SMA-tanespimycin micelles was also significantly reduced as compared to tanespimycin formulated in EtOH:CrEL:PEG at all time points greater than 1 h ($p < 0.001$), with only 62% release observed in 24 h (Fig. 3). This reduction in release rate can be explained by the well characterized noncovalent binding of SMA to serum albumin (Kobayashi et al., 1988), and it is thus anticipated that serum albumin can serve as a secondary carrier for SMA-tanespimycin micelles *in vivo*.

3.4. Cytotoxicity of SMA-tanespimycin micelles in vitro

The ability of SMA-tanespimycin micelles to inhibit the growth of DU145 human prostate cancer cells was evaluated *in vitro* using a WST-8 cell viability assay. Incorporation of tanespimycin into SMA-tanespimycin micelles resulted in a decrease in its ability to inhibit the growth of DU145 cells with an IC_{50} of 230 ± 10 nM as compared to an IC_{50} of 15.0 ± 0.3 nM for tanespimycin solubilized in EtOH:CrEL:PEG (Fig. 4). For controls, SMA and EtOH:CrEL:PEG solutions were subjected to the same dilution protocol and evaluated for growth inhibition ability and showed no cytotoxicity over an equivalent concentration range. During the 72 h incubation time of these studies, the release of tanespimycin from SMA-tanespimycin micelles was most likely minimized because of the lack of a perpetual sink condition. Although SMA-tanespimycin micelles were less toxic as compared to free tanespimycin, they remained cytotoxic in the nanomolar concentration range. This reduction in cytotoxicity of SMA-tanespimycin micelles as compared to free tanespimycin can be explained by a number of possible factors. The micelles first need to be taken up by cells via endocytosis, whereas tanespimycin can passively diffuse across cellular membranes. Uptake of the micelles could further be reduced due to the interactions of the negatively charged carboxylic acid rich surface of the micelles with negatively charged membranes. Tanespimycin must also be released from the micelle core in order for it to elicit its pharmacological effect, which occurs over a prolonged time interval, further reducing overall cytotoxic exposure. The reduced toxicity of SMA-tanespimycin micelles can potentially be advantageous in an *in vivo* scenario by minimizing systemic exposure of tanespimycin while allowing time for accumulation in tumor tissues to occur.

3.5. In vivo efficacy of SMA-tanespimycin micelles

The delivery of tanespimycin via SMA-tanespimycin micelles results in an increase in the therapeutic index for tanespimycin. Toward this aim, a preliminary *in vivo* efficacy study was performed in athymic nu/nu mice bearing subcutaneous DU145 human prostate cancer xenografts. As accumulation in tumor tissues via the EPR effect was anticipated for SMA-tanespimycin micelles, a subtherapeutic dose of 10 mg/kg tanespimycin equivalent was used. A single dose of SMA-tanespimycin micelles, free tanespimycin, or saline were injected via tail-vein injection and animals were monitored twice weekly for changes in tumor volume as an indicator of efficacy (Fig. 5). Body weight was also recorded as an indicator of general toxicity (Fig. 5). At a single dose of 10 mg/kg tanespimycin equivalent, SMA-tanepsimycin micelles resulted in a reduction in normalized mean tumor volume that was maintained throughout the duration of the study (23 days), whereas

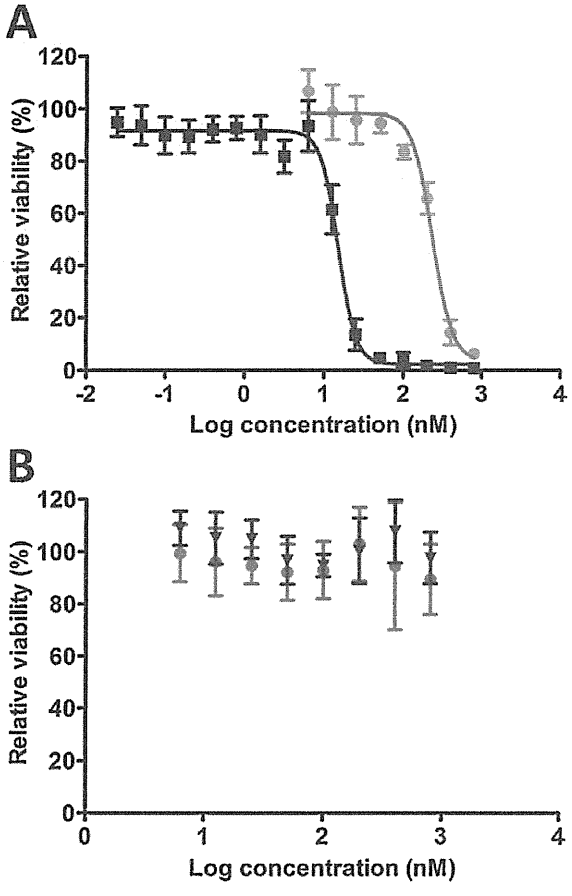

Fig. 4. Cell growth inhibition of SMA-tanespimycin micelles. DU145 human prostate cancer cells were treated for 72 h with increasing drug equivalent concentrations of tanespimycin formulated in EtOH:CrEL:PEG (blue), SMA-tanespimycin micelles (red) (A), EtOH:CreEL:PEG vehicle alone (blue) or hydrolyzed SMA (red) (B). Following treatment, cell viability was assessed by WST-8 assay. Non-linear regression and IC_{50} values were determined by analysis using GraphPad Prism. (For interpretation of the references to color in the figure caption, the reader is referred to the web version of the article.)

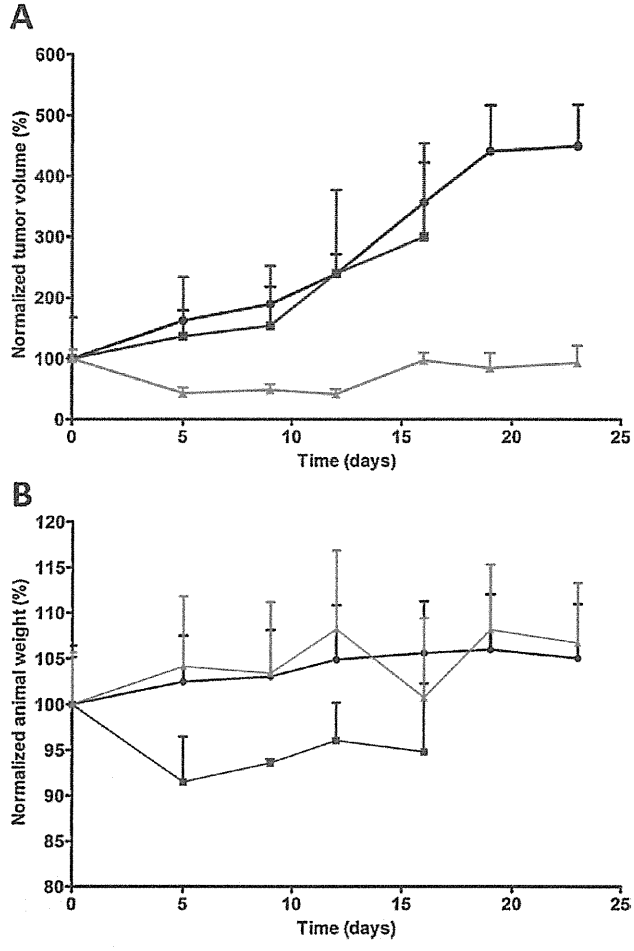

Fig. 5. *In vivo* efficacy of SMA-tanespimycin micelles. Athymic nu/nu mice bearing DU145 tumor xenografts were treated IV with a single dose of 10 mg/kg tanespimycin (blue) or 10 mg/kg tanespimycin equivalent SMA-tanespimycin micelles (red) and compared with a saline injection control group (black). (A) Normalized tumor volume was measured as a function of time for each treatment group. (B) Normalized animal weight was assessed as a measure of general toxicity. Data are expressed as mean ± SEM ($N = 5$ per treatment group). *Difference detected at $p < 0.05$ significance level. (For interpretation of the references to color in the figure caption, the reader is referred to the web version of the article.)

normalized mean tumor volume in saline injected animals increased 450%. Relative to saline injected animals, SMA-tanespimycin resulted in a statistically significant decrease in normalized mean tumor volume at all time points following treatment ($p < 0.05$). A single dose of free tanespimycin showed no evidence of efficacy at 10 mg/kg, and normalized mean tumor volume was not different from saline injected animals at all time points. Animals in the free tanespimycin group were euthanized on day 16 as one animal showed excessive tumor burden. SMA-tanespimycin micelles in comparison with free tanespimycin showed a significant reduction in normalized mean tumor volume on day 16 ($p < 0.05$). These results coupled with the *in vitro* cytotoxicity results suggest that SMA-tanespimycin micelles have the ability to accumulate in tumor tissues and inhibit tumor growth *in vivo*.

Animal weights were measured twice a week as an indicator of general toxicity during the efficacy study. Relative to saline injected animals, animals treated with SMA-tanespimycin micelles showed no difference in normalized mean animal weight during the study. An 11% reduction in normalized mean animal weight was observed for free tanespimycin as compared to saline injected animals at day 5 ($p < 0.05$); differences detected at subsequent time points were not statistically significant. However, it is unclear whether the solvent used to solubilize tanespimycin has contributed to the overt tanespimycin toxicity in this study, or the manifested toxicity was totally due to the free drug. These results demonstrate that SMA-tanespimycin micelles were well tolerated.

This efficacy study was preliminary in its nature as parameters such as maximum tolerated dose and dosing schedule were not optimized. However, the results of the study demonstrate that SMA-tanespimycin micelles were well tolerated and effective in reducing DU145 tumor growth, and suggest that the therapeutic index of tanespimycin is increased by encapsulation in SMA micelles.

Overall, the data from this study demonstrates that delivery of tanespimycin using SMA micelles has several distinct advantages. First, the aqueous solubility of tanespimycin is increased by encapsulation into SMA micelles, and because these interactions are non-covalent, the potent activity of tanespimycin is maintained. Second, the preparation of SMA-tanespimycin micelles is simple, straightforward, and efficient in loading tanespimycin, thus allowing cost efficient scale up at later stages of development. Third, the macromolecular nature of SMA-tanespimycin micelles allows accumulation into tumor tissues, resulting in an increase in the therapeutic index of tanespimycin. These features combine to suggest that SMA-tanespimycin micelles have the potential to increase the efficacy and safety profile of tanespimycin.

4. Conclusion

SMA-tanespimycin micelles were prepared in a simple manner with a high loading drug efficiency of 93%. The micelles incorporated 25.6% tanespimycin by weight and exhibited properties that allow for increased blood circulation and tumor accumulation *in vivo*. Tanespimycin was released from the micelles in a controlled manner and showed potent activity against DU145 human prostate cancer cells *in vitro*. The micelles also were well tolerated and exhibited potent anti-cancer activity in nu/nu mice bearing subcutaneous DU145 human prostate cancer tumor xenografts, with a significant increase in efficacy as measured by tumor regression as compared to free tanespimycin at an equivalent single dose of 10 mg/kg. These data suggest that the therapeutic index of tanespimycin is increased by incorporation into SMA micelles.

Acknowledgements

This research was supported by the National Institutes of Health grant R01 EB007171 and the Utah Science Technology and Research (USTAR) initiative.

References

Banerji, U., O'donnell, A., Scurr, M., Pacey, S., Stapleton, S., Asad, Y., Simmons, L., Maloney, A., Raynaud, F., Campbell, M., Walton, M., Lakhani, S., Kaye, S., Workman, P., Judson, I., 2005. Phase I pharmacokinetic and pharmacodynamic study of 17-allylamino, 17-demethoxygeldanamycin in patients with advanced malignancies. J. Clin. Oncol. 23, 4152–4161.

Blanco, E., Kessinger, C.W., Sumer, B.D., Gao, J., 2009. Multifunctional micellar nanomedicine for cancer therapy. Exp. Biol. Med. 234, 123–131.

Borgman, M.P., Aras, O., Geyser-Stoops, S., Sausville, E.A., Ghandehari, H., 2009. Biodistribution of HPMA copolymer-aminohexylgeldanamycin-RGDfK conjugates for prostate cancer drug delivery. Mol. Pharm. 6, 1836–1847.

Buchner, J., 1999. Hsp90 & Co.—a holding for folding. Trends Biochem. Sci. 24, 136–141.

Burger, A.M., Fiebig, H.H., Stinson, S.F., Sausville, E.A., 2004. 17-(Allylamino)-17-demethoxygeldanamycin activity in human melanoma models. Anticancer Drugs 15, 377–387.

Claracq, J., Santos, S.F.C.R., Duhamel, J., Dumousseaux, C., Corpart, J.-M., 2002. Rigid interior of styrene–maleic anhydride copolymer aggregates probed by fluorescence spectroscopy. Langmuir 18, 3829–3835.

Croy, S.R., Kwon, G.S., 2006. Polymeric micelles for drug delivery. Curr. Pharm. Des. 12, 4669–4684.

Daruwalla, J., Nikfarjam, M., Greish, K., Malcontenti-Wilson, C., Muralidharan, V., Christophi, C., Maeda, H., 2010. In vitro and in vivo evaluation of tumor targeting styrene–maleic acid copolymer-pirarubicin micelles: survival improvement and inhibition of liver metastases. Cancer Sci. 101, 1866–1874.

Fukuyo, Y., Hunt, C.R., Horikoshi, N., 2010. Geldanamycin and its anti-cancer activities. Cancer Lett. 290, 24–35.

Gaucher, G., Dufresne, M.H., Sant, V.P., Kang, N., Maysinger, D., Leroux, J.C., 2005. Block copolymer micelles: preparation, characterization and application in drug delivery. J. Control. Release 109, 169–188.

Ge, J., Normant, E., Porter, J.R., Ali, J.A., Dembski, M.S., Gao, Y., Georges, A.T., Grenier, L., Pak, R.H., Patterson, J., Sydor, J.R., Tibbitts, T.T., Tong, J.K., Adams, J., Palombella, V.J., 2006. Design, synthesis, and biological evaluation of hydroquinone derivatives of 17-amino-17-demethoxygeldanamycin as potent, water-soluble inhibitors of Hsp90. J. Med. Chem. 49, 4606–4615.

Gelderblom, H., Verweij, J., Nooter, K., Sparreboom, A., 2001. Cremophor® EL: the drawbacks and advantages of vehicle selection for drug formulation. Eur. J. Cancer 37, 1590–1598.

Greish, K., 2007. Enhanced permeability and retention of macromolecular drugs in solid tumors: a royal gate for targeted anticancer nanomedicines. J. Drug Target 15, 457–464.

Greish, K., Fang, J., Inutsuka, T., Nagamitsu, A., Maeda, H., 2003. Macromolecular therapeutics: advantages and prospects with special emphasis on solid tumour targeting. Clin. Pharmacokinet. 42, 1089–1105.

Greish, K., Sawa, T., Fang, J., Akaike, T., Maeda, H., 2004. SMA-doxorubicin, a new polymeric micellar drug for effective targeting to solid tumours. J. Control. Release 97, 219–230.

Gros, L., Ringsdorf, H., Schupp, H., 1981. Polymeric antitumor agents on a molecular and on a cellular level? Angew. Chem. Int. Ed. Engl. 20, 305–325.

Iyer, A.K., Greish, K., Fang, J., Murakami, R., Maeda, H., 2007. High-loading nanosized micelles of copoly(styrene-maleic acid)-zinc protoporphyrin for targeted delivery of a potent heme oxygenase inhibitor. Biomaterials 28, 1871–1881.

Kasuya, Y., Lu, Z.R., Kopeckova, P., Tabibi, S.E., Kopecek, J., 2002. Influence of the structure of drug moieties on the in vitro efficacy of HPMA copolymer-geldanamycin derivative conjugates. Pharm. Res. 19, 115–123.

Kelland, L.R., Sharp, S.Y., Rogers, P.M., Myers, T.G., Workman, P., 1999. DT-diaphorase expression and tumor cell sensitivity to 17-allylamino, 17-demethoxygeldanamycin, an inhibitor of heat shock protein 90. J. Natl. Cancer Inst. 91, 1940–1949.

Kobayashi, A., Oda, T., Maeda, H., 1988. Protein binding of macromolecular anticancer agent SMANCS: characterization of poly(styrene-co-maleic acid) derivatives as an albumin binding ligand. J. Bioact. Compat. Polym. 3, 319–333.

Larson, N., Ray, A., Malugin, A., Pike, D.B., Ghandehari, H., 2010. HPMA copolymer-aminohexylgeldanamycin conjugates targeting cell surface expressed GRP78 in prostate cancer. Pharm. Res. 27, 2683–2693.

Maeda, H., 2001. SMANCS and polymer-conjugated macromolecular drugs: advantages in cancer chemotherapy. Adv. Drug Deliv. Rev. 46, 169–185.

Matsumura, Y., Oda, T., Maeda, H., 1987. General mechanism of intratumor accumulation of macromolecules: advantage of macromolecular therapeutics. Gan To Kagaku Ryoho 14, 821–829.

Park, K., 2007. Nanotechnology: what it can do for drug delivery. J. Control. Release 120, 1–3.

Porter, J.R., Ge, J., Lee, J., Normant, E., West, K., 2009. Ansamycin inhibitors of Hsp90: nature's prototype for anti-chaperone therapy. Curr. Top. Med. Chem. 9, 1386–1418.

Rodriguez, V.B., Henry, S.M., Hoffman, A.S., Stayton, P.S., Li, X., Pun, S.H., 2008. Encapsulation and stabilization of indocyanine green within poly(styrene-alt-maleic anhydride) block-poly(styrene) micelles for near-infrared imaging. J. Biomed. Opt. 13, 014025.

Rowinsky, E.K., Donehower, R.C., 1995. Paclitaxel (taxol). N. Engl. J. Med. 332, 1004–1014.

Sausville, E.A., Tomaszewski, J.E., Ivy, P., 2003. Clinical development of 17-allylamino, 17-demethoxygeldanamycin. Curr. Cancer Drug Targets 3, 377–383.

Sharp, S., Workman, P., 2006. Inhibitors of the HSP90 molecular chaperone: current status. Adv. Cancer Res. 95, 323–348.

Shin, H.-C., Alani, A.W.G., Rao, D.A., Rockich, N.C., Kwon, G.S., 2009. Multi-drug loaded polymeric micelles for simultaneous delivery of poorly soluble anticancer drugs. J. Control. Release 140, 294–300.

Subr, V., Kopecek, J., Pohl, J., Baudys, M., Kostka, V., 1988. Cleavage of oligopeptide side-chains in N-(2-hydroxypropyl)methacrylamide copolymers by mixtures of lysosomal enzymes. J. Control. Release 8, 133–140.

Supko, J.G., Hickman, R.L., Grever, M.R., Malspeis, L., 1994. Preclinical pharmacologic evaulation of geldanamycin as an antitumor agent. Cancer Chemother. Pharmacol. 36, 305–315.

Suzuki, F., Munakata, T., Maeda, H., 1988. Interferon induction by SMANCS: a polymer-conjugated derivative of neocarzinostatin. Anticancer Res. 8, 97–103.

Suzuki, F., Pollard, R.B., Uchimura, S., Munakata, T., Maeda, H., 1990. Role of natural killer cells and macrophages in the nonspecific resistance to tumors in mice stimulated with SMANCS, a polymer-conjugated derivative of neocarzinostatin. Cancer Res. 50, 3897–3904.

Whitesell, L., Lindquist, S.L., 2005. HSP90 and the chaperoning of cancer. Nat. Rev. Cancer 5, 761–772.

Xiong, M.P., Yáñez, J.A., Kwon, G.S., Davies, N.M., Forrest, M.L., 2009. A cremophor-free formulation for tanespimycin (17-AAG) using PEO-*b*-PDLLA micelles: characterization and pharmacokinetics in rats. J. Pharm. Sci. 98, 1577–1586.

Zhong, Z., Licari, P.J., 2005. Pharmaceutical solution formulations containing 17-AAG. US Patent Application, 20,050,256,097.

tapraid3/zpt-pt/zpt-pt/zpt01211/zpt9629d11z | xppws | S=1 | 10/22/11 | 15:56 | 4/Color Figure(s): 6,8 | Art: 185348 | Input-KAF

0022-3565/11/3393-1–11$25.00
THE JOURNAL OF PHARMACOLOGY AND EXPERIMENTAL THERAPEUTICS
Copyright © 2011 by The American Society for Pharmacology and Experimental Therapeutics
JPET 339:1–11, 2011

Vol. 339, No. 3
185348/3729805
Printed in U.S.A.

Therapeutic Potential of Pegylated Hemin for Reactive Oxygen Species-Related Diseases via Induction of Heme Oxygenase-1: Results from a Rat Hepatic Ischemia/Reperfusion Injury Model[S]

Jun Fang, Haibo Qin, Takahiro Seki,[1] Hideaki Nakamura, Kenji Tsukigawa, and Hiroshi Maeda

Laboratory of Microbiology and Oncology, Faculty of Pharmaceutical Sciences (J.F., H.Q., T.S., H.N., K.T.), Department of Applied Microbial Technology, Faculty of Biotechnology and Life Science (H.Q.), and DDS Research Institute (H.N., H.M.), Sojo University, Kumamoto, Japan

Received June 23, 2011; accepted September 2, 2011

ABSTRACT

AQ: A Many diseases and pathological conditions, including ischemia/reperfusion (I/R) injury, are the consequence of the actions of reactive oxygen species (ROS). Controlling ROS generation or its level may thus hold promise as a standard therapeutic modality for ROS-related diseases. Here, we assessed heme oxygenase-1 (HO-1), which is a crucial antioxidative, antiapoptotic molecule against intracellular stresses, for its therapeutic potential via its inducer, hemin. To improve the solubility and in vivo pharmacokinetics of hemin for clinical applications, we developed a micellar hemin by conjugating it with poly(ethylene glycol) (PEG) (PEG-hemin). PEG-hemin showed higher solubility in water and significantly prolonged plasma half-life than free hemin, which resulted from its micellar nature with molecular mass of 126 kDa in aqueous media. In a rat I/R model, administration of PEG-hemin significantly elevated HO-1 expression and enzymatic activity. This induction of HO-1 led to significantly improved liver function, reduced apoptosis and thiobarbituric acid reactive substances of the AQ: B liver, and decreased inflammatory cytokine production. PEG-hemin administration also markedly improved hepatic blood flow. These results suggest that PEG-hemin exerted a significant cytoprotective effect against I/R injury in rat liver by inducing HO-1 and thus seems to be a potential therapeutic for ROS-related diseases, including I/R injury.

Introduction

All aerobic organisms generate reactive oxygen species (ROS), which seem to be indispensable for signal transduction pathways that regulate cell growth and redox status (Davies, 1995). However, overproduction of these highly reactive metabolites can initiate lethal chain reactions and damage cell integrity and survival (Oda et al., 1989; Davies, 1995), which result in reversible and irreversible tissue injury. ROS are known to be involved in many diseases, for example, microbial infections, inflammation, ischemia/reperfusion (I/R) injury, neurological disorders, Parkinson's disease, hypertension, and cancer (Maeda and Akaike, 1991; McCord, 2000). Developing therapeutics for these ROS-related diseases by suppressing ROS generation or its levels in the body therefore seems to be a reasonable approach. Indeed, many research groups have used this rationale and

This work was supported in part by the Ministry of Education, Science, Culture, Sports, and Technology of Japan [Grants-in-Aid 17016076, 20015405]; and research funds from the Faculty of Pharmaceutical Sciences at Sojo University.

Part of this work was presented previously: Fang J, Qin H, Seki T, Nakamura H, Bharate GY, and Maeda H (2010) Pegylated hemin, a water-soluble micelle with therapeutic potential against ischemia-reperfusion injury via induction of heme oxygenase-1, at the *37th Annual Meeting and Exposition of the Controlled Release Society*; 2010 July 10–14; Portland, OR. Controlled AQ: V Release Society, St. Paul, MN.

J.F. and H.Q. contributed equally to this work.

[1]Current affiliation: Laboratory of Angiogenesis Research, Department of Microbiology, Tumor and Cell Biology, Karolinska Institute, Stockholm, Sweden.

Article, publication date, and citation information can be found at http://jpet.aspetjournals.org.
doi:10.1124/jpet.111.185348.

[S] The online version of this article (available at http://jpet.aspetjournals.org) contains supplemental material.

ABBREVIATIONS: ROS, reactive oxygen species; HO, heme oxygenase; XO, xanthine oxidase; PEG, poly(ethylene glycol); EPR, enhanced permeability and retention; I/R, ischemia/reperfusion; TBARS, thiobarbituric acid reactive substance; PCR, polymerase chain reaction; ZnPP, zinc protoporphyrin; DLS, dynamic light scattering; AUC, area under the concentration versus time curve; Hc, hepatocytes; GAPDH, glyceraldehyde-3-phosphate dehydrogenase; SMA, styrene maleic acid; ALT, alanine aminotransferase; AST, aspartate aminotransferase; LDH, lactate dehydrogenase; TUNEL, terminal deoxynucleotidyl transferase dUTP nick-end labeling; 8-OHdG, 8-hydroxydeoxyguanosine; ELISA, enzyme-linked AQ: W immunosorbent assay; MCP-1, monocyte chemotactic protein 1.

investigated various antioxidative agents and enzymes, such as superoxide dismutase and catalase (Oda et al., 1989; Muzykantov et al., 1996; Fang et al., 2009b). Inhibitors of the ROS-generating enzyme xanthine oxidase (XO) were also the targets along this line (Miyamoto et al., 1996; Fang et al., 2009a, 2010).

In addition to these enzymes, heme oxygenase-1 (HO-1), the antioxidative, antiapoptotic molecule, has attracted great attention. HO is the key enzyme in heme degradation, which generates biliverdin, carbon monoxide (CO), and free iron (Fe^{2+}) (Maines, 1988; Fang et al., 2004). Biliverdin is subsequently reduced by cytosolic biliverdin reductase to form bilirubin, a potent antioxidant (Baranano et al., 2002). In addition, reports have shown that CO contributes in regulating vascular tone and exhibits antioxidative, anti-inflammatory, and antiapoptotic properties (Abraham and Kappas, 2008). HO-1 is the inducible form of HO, which is a member of the heat shock protein family (Hsp32), and its expression is believed to be associated with fundamental adaptive and defensive responses to oxidative stress and cell stress (Doi et al., 1999; Fang et al., 2004; Abraham and Kappas, 2008). Therefore, induction of HO-1 may become an effective therapeutic strategy for ROS-related diseases. Among HO-1 inducers, hemin is one of the most potent and has few adverse effects to the host. In fact, hemin is used to treat acute hepatic porphyria in Europe and the United States.

However, the very poor water solubility of hemin makes it difficult to achieve a clinically effective dose and develop an optimal therapeutic protocol. To overcome this drawback, we prepared a water-soluble micellar form of hemin by using the biocompatible polymer poly(ethylene glycol) (PEG) (PEG-hemin). This polymer conjugation resulted in an increased in vivo half-life ($t_{1/2}$) and reduced antigenicity, as reported previously (Sawa et al., 2000; Fang et al., 2003), and improves pharmacological efficacy significantly.

I/R injury, a typical ROS-related pathological process, is a major cause of organ damage in many fatal diseases such as cardiac infarction, cerebral ischemia, and thrombosis, as well as in surgical procedures. Many studies reported that ROS, especially superoxide anion radical (O_2^-), is produced excessively in many tissues, mostly by XO, during I/R injury (McCord, 1985). Under normal conditions most XO is present as xanthine dehydrogenase type D, which has very low O_2^--generating activity; however, during ischemia, XO activity rapidly increases by conversion from XO type D to type O, which leads to rapid production of O_2^- (Roy and McCord, 1983). O_2^-, with highly cytotoxic activity, is converted to H_2O_2 by superoxide dismutase, and then to hydroxyl radicals in the presence of transition metals (e.g., Fe^{2+}), if no catalase is available. All of these ROS can readily cross cell membranes and cause oxidative damage to DNA, proteins, and lipids (Halliwell and Gutteridge, 1984; Beckman and Ames, 1997; Berlett and Stadtman, 1997). In addition, O_2^- can react rapidly with NO and form the more toxic species peroxynitrite ($ONOO^-$), which further exacerbates tissue injury or leads to complications. Furthermore, removal of NO by reactions with O_2^- on the vascular endothelial surface results in vasoconstriction (hypertension) and triggers neutrophil adherence and accumulation, which will exacerbate reperfusion injury (Beckman and Koppenol, 1996; Akaike and Maeda, 2000). All of these data together indicate that ROS are the major cause of I/R-induced tissue injury and subsequent pathological manifestations.

The present study describes the synthesis of PEG-hemin and the physicochemical and biological characterization of the conjugate. In view of the therapeutic potential of this agent for ROS-related diseases, this study also evaluated the cytoprotective effect of PEG-hemin in vivo in a rat liver I/R model.

Materials and Methods

Materials. Hemin was purchased from Sigma-Aldrich (St. Louis, MO). The succinimidyl glutarate derivative of PEG (MEGC-50HS), with a mean molecular weight of 5250, was from NOF Co. (Tokyo, Japan). PEG used in this experiment had a molecular weight dispersity index of 1.025. Other chemicals of reagent grade were from Wako Pure Chemicals (Osaka, Japan) and used without additional purification.

Cell Culture. Human hepatocyte Hc cells (DS Pharma Biomedical Co. Ltd, Osaka, Japan) were cultured in CSC Serum-Free Medium (DS Pharma Biomedical Co. Ltd) at 37°C in a 5% CO_2/95% air atmosphere.

Animals. Male Wistar rats, 6 to 7 weeks old and weighing between 200 and 230 g, and 6-week-old male *ddY* mice, weighing between 20 and 25 g, were obtained from Kyudo Inc. (Kumamoto, Japan). All animals were maintained under standard conditions and fed water and murine chow ad libitum. All experiments were carried out according to the guidelines of the Laboratory Protocol of Animal Handling, Faculty of Pharmaceutical Sciences, Sojo University.

Synthesis of PEG-Hemin. PEG-hemin was synthesized according to the protocol for PEG-zinc protoporphyrin (PEG-ZnPP) synthesis described in our previous work (Sahoo et al., 2002), with some modifications. In brief, an aminated derivative of hemin was synthesized by using ethylenediamine, and then succinimidyl PEG was cross-linked to hemin via the amide bond (Scheme 1). The resultant PEG-hemin was characterized by means of a UV spectrophotometer (model UV/Vis-550; Jasco, Tokyo, Japan) and infrared spectrometer (FT/IR-4200; Jasco), as well as dynamic light scattering (DLS) and Sephadex column chromatography, as described below.

Quantification of the Free Amino Group. To determine whether PEG reacted with the amino group introduced into hemin, loss of the primary amino group after the reaction was quantified by the use of fluorescamine, an amino group-reactive fluorescent agent (Stocks et al., 1986). In brief, 2 μM PEG-hemin (hemin equivalent) and diethylaminohemin (aminated derivative of hemin) were dissolved in deionized water and then reacted with fluorescamine. Fluorescence was detected at 475 nm with excitation at 390 nm. The concentration of free amino groups in PEG-hemin was estimated by using glycine as the standard.

Size Exclusion Chromatography. Size exclusion chromatography was performed with a Sephadex G-100 column, 40 cm (length) × 1.3 cm (diameter) (GE Healthcare, Chalfont St. Giles, Buckinghamshire, UK), to determine the apparent molecular mass of PEG-hemin. Various globular proteins of known molecular mass were used as reference standards. The mobile phase was 0.25 M $NaHCO_3$, pH 8.2, and 2.5-ml fractions were collected per tube.

DLS Measurement of PEG-Hemin Particle Size. DLS measurement was performed with the Photal DLS-7000 HLs laser spectrophotometer (Otsuka Electronics, Osaka, Japan), equipped with a 10-mW He/Ne laser, at a wavelength of 632.8 nm. The scattering angle was fixed at 90°, and the temperature was at 25°C ± 0.05°C. Particle size was determined with 0.1 mg/ml samples prepared in deionized water (filtered through a 0.45-μm filter).

In Vivo Pharmacokinetics of PEG-Hemin. *ddY* mice were used in the determination of PEG-hemin plasma $t_{1/2}$, area under the concentration versus time curve (AUC), and total body clearance. PEG-hemin (dissolved in physiological saline) or free hemin (dissolved in 0.01 M NaOH with 10% dimethyl sulfoxide) was injected intravenously at 10 mg/kg (hemin equivalent). After scheduled in-